LAWRENCE
LIVERMORE
NATIONAL
LABORATORY

LLNL-JRNL-665610

Highly Charged Ions in Magnetic Fusion Plasmas: Research Opportunities and Diagnostic Necessities

P. Beiersdorfer

December 22, 2014

Journal of Physics B

Disclaimer

Highly Charged Ions in Magnetic Fusion Plasmas: Research Opportunities and Diagnostic Necessities

P. Beiersdorfer

Physics Department, Lawrence Livermore National Laboratory, Livermore, CA 94550, USA

E-mail: beiersdorfer@llnl.gov

Abstract.

Highly charged ions play a crucial role in magnetic fusion plasmas. These plasmas are excellent sources for producing highly charged ions and copious amounts of radiation for studying their atomic properties. These studies include calibration of density diagnostics, x-ray production by charge exchange, line identifications and accurate wavelength measurements, and benchmark data for ionization balance calculations. Studies of magnetic fusion plasmas also consume a large amount of atomic data, especially in order to develop new spectral diagnostics. Examples we give are the need for highly accurate wavelengths as references for measurements of bulk plasma motion, the need for accurate line excitation rates that encompass both electron-impact excitation and indirect line formation processes, for accurate position and resonance strength information of dielectronic recombination statellite lines that may broaden or shift diagnsotic lines or that may provide electron temperature information, and the need for accurate ionization balance calculations. We show that the highly charged ions of several elements are of special current interest to magnetic fusion, notably highly charged tungsten ions. The electron temperatures thought to be achievable in the near future may produce W^{70+} ions and possibly ions with even higher charge states. This means that all but a few of the most highly charged ions are of potential interest as plasma diagnostics or are available for basic research.

1. Introduction

Present-day magnetic fusion devices, especially tokamaks, can generate plasmas with electron temperatures near 10 keV, and future machines may even reach temperatures in excess of 25 keV. This means that they can produce ions with very high charge even from heavy elements. From the beginning, highly charged ions have constituted an important component of magnetically confined plasmas, and their presence has been both highly advantageous, for example, for plasma diagnostics and basic atomic physics studies, and detrimental to the function of a given device, if present in large quantities.

The good and bad properties of highly charged ions derive from the fact that they radiate when embedded in a sea of electrons. Partially ionized heavy elements radiate profusely, mostly in the extreme ultraviolet wavelength range, while ions stripped

to a few electrons within a closed shell, such heliumlike or neonlike ions, radiate predominantly in the x-ray range. This radiation can be used to diagnose the plasma conditions, such as the electron temperature, electron density, ion temperature, ion transport and diffusion, and bulk plasma motion. The radiation from highly charged ions contributes to the overall power loss of the plasma, and the associated radiative power loss can be severe and prevent ignition and burn, if the plasma contains too many heavy ions. Even fully stripped, i.e. bare, ions of light elements contribute to the radiative power loss via the radiative capture of free electrons and via Bremsstrahlung. Thus, even bare ions of beryllium, boron, carbon, or oxygen, are detrimental to achiving fusion, if they are present in too high concentrations.

Nowadays, magnetic fusion devices aim to strictly limit the presence of highly charged ions in the plasma. Plasma-facing components are made of or are coated with carbon or boron, sometimes even beryllium or lithium in order to eliminate the influx of aluminum, iron, copper, or molybdenum, which was seen in the past. This means that sometimes high-Z ions are deliberately (re-)introduced into the plasma, albeit in a highly controlled way by means of laser blow-off [1] or so-called tracer-encapsulated solid pellet (TESPEL) injection [2], in order to take advantage of the diagnostic utilities afforded by highly charged ions.

The trend of magnetically confined plasmas containing fewer highly charged ions has been broken in light of the impending operation of the ITER (Latin, 'the way') tokamak, which is under construction in Cadarache, France, and which is designed to produce a substantial amount of energy from nuclear fusion [3]. The high heat load impinging on plasma facing components requires the use of materials with a high melting point. Moreover, the material must not absorb hydrogen; specifically, it cannot absorb tritium, which, being a radioactive material, is in short supply because of regulatory controls associated with ITER operation. The only practical material under consideration that meets these critera is tungsten, and it is, therefore, planned to build the plasma divertor out of this high-Z material ($Z = 74$).

Plasma striking the ITER divertor plates will sputter tungsten, and some of it will diffuse into the main plasma region. ITER design assumes a tungsten concentration of $\leq 1 \times 10^{-5}$. This much less than the assumed concentration of beryllium ($\leq 2 \times 10^{-2}$) or argon ($\leq 1 \times 10^{-3}$), but the concentration of all other elements heavier than argon is assumed to be zero. Although there are discussions to permit possibly stainless steel as a first wall material in a few places [4], for the time being, tungsten will be the only indigenous heavy element in ITER.

Tungsten is by far the heaviest element used in magnetic fusion, and the use of tungsten in the design of ITER has added a new dimension to the importance of highly charged ion research. In preparation for ITER, many present-day machines have started to use "ITER-like" plasma facing components, i.e. tungsten or molybdenum. As a result, these machines now contain a newly found abundance of highly charged heavy ions. The electron temperatures in these machines produce tungsten ions in excess of nickellike (W^{46+}); the colder plasma regions are dominated by partially filled N-

shell tungsten ions, for which there is precious little atomic data. This has recently spurred many experimental and theoretical investigations of open-shell tungsten ions [5, 6, 7, 8, 9, 10, 11, 12, 13, 14, 15, 16, 17, 18, 19, 20, 21, 22].

The electron temperatures in ITER are envisioned to reach about 30 keV, which means that tungsten ions with a partially filled M-shell abound in these hotter plasma, and in the hottest core tungsten ions may become neonlike (W^{64+}) and beyond. The prospect of having very highly charged ions in the ITER core has spurred the design of the US core-imaging x-ray crystal spectrometer (CIXS) based on the L-shell x-ray lines from neonlike tungsten and lines from the closest neighboring ions [23]. This in turn requires a better understanding of the atomic physics associated with the L-shell emission of such highly charged tungsten ions.

The focus on tungsten and its many charge states radiating in wavelength bands from the visible to the x-ray regime coupled with the prospect of plasmas with much higher electron temperature than achievable in the past gives new opportunities for research of highly charged ions. New diagnostic lines need to be developed in order to determine, for example, impurity transport, ion temperatures, and toroidal rotation velocities. New atomic data needs to be generated in support of developing such diagnostic, which may include line identifications, accurate wavelength measurements, and excitation cross section measurements. As a result, ancillary studies of tungsten ions beyond those performed on magnetic fusion devices are necessary. In addition, atomic physics measurements may be performed directly on fusion machines, as these devices give access to plasma regimes not afforded by other research facilities such as heavy-ion storage rings or electron beam ion traps. In the following we discuss the need for measurements of tungsten and the possibility of using fusion devices for highly charged ion research in detail. We will emphasize x-ray measurements, but much of this discussion can easily be extended to measurements in other wavelength bands.

The paper is organized as follows. In the next Section we will give a brief overview of the plasma conditions found in tokamaks. This is followed by a discussion of the uses of highly charged ions for plasma diagnostics. Using the requirements of the CIXS on ITER as an example, we delineate the atomic data needed for optimizaing the science return of this diagnostic in Section 4. Finally, in Section 5, we illustrate the use of magnetic fusion devices for studying highly charged ions.

2. Plasma Conditions

About thirty years ago, the Princeton Large Torus (PLT) tokamak was optimized to produced high electron temperatures in order to allow the studies of highly charged ions of heavy elements, the highest of which was neonlike Eu^{53+} [24, 25]. PLT was a medium-sized tokamak with a plasma diameter of about 80 cm, plasma currents up to 650 kA, and toroidal magnetic fields of about 3 T. Typical time histories of the discharge parameters are shown in Fig. 1, and typical electron temperature and electron density profiles profiles are shown in Figs. 2 and 3, respectively.

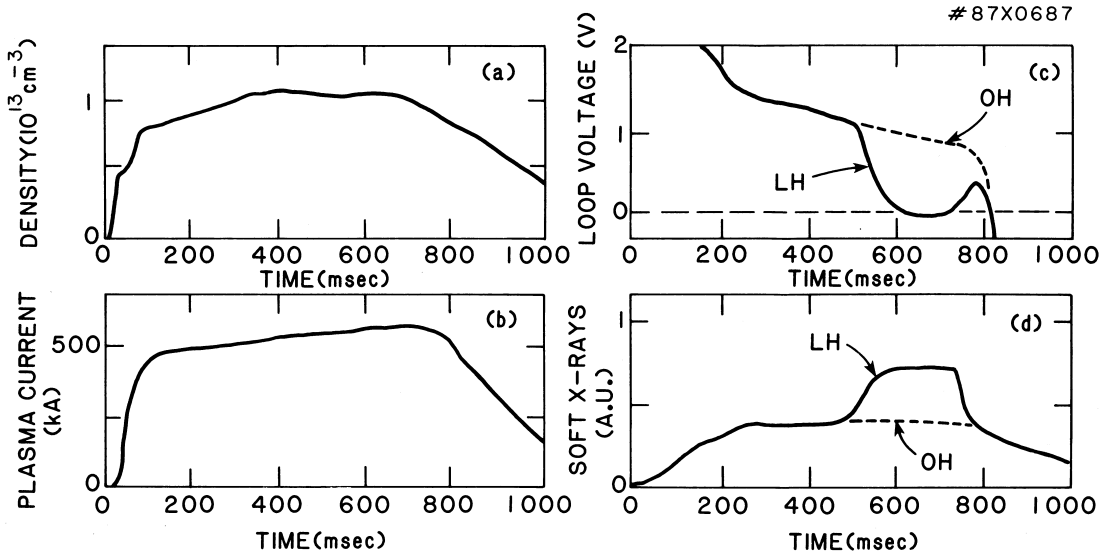

Figure 1. Time evolution of the discharge parameters on PLT for both ohmically heated plasmas (OH) and plasmas with lower hybrid wave injection (LH): (a) electron density, (b) plasma current, (c) loop voltage, soft x-ray emission.

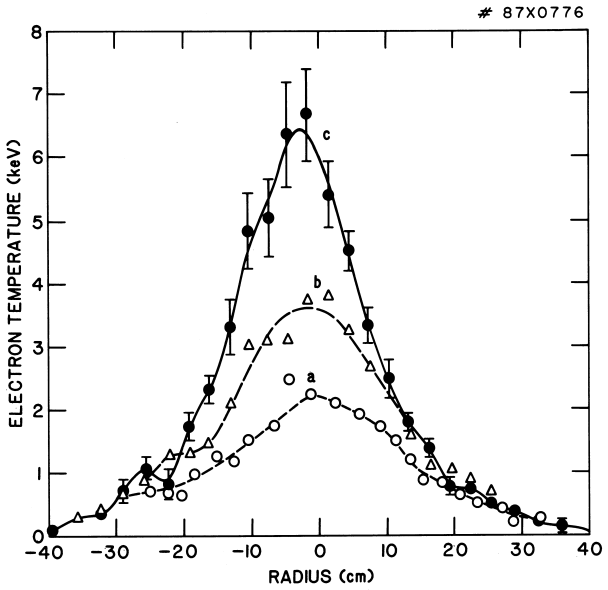

Figure 2. Electron temperature profiles of PLT plasmas measured with the Thomson scattering diagnostic: (a) ohmically heated plasma, (b) plasma seeded with neon to increase Z_{eff}, (c) plasma heated with additional lower hybrid wave injection.

The peak electron temperatures achieved in the PLT experiments approached about 7 keV. These were among the highest achieved by any such device, including present-day machines, even those that are much larger than PLT. The reason is not that the

large machines, such as the DIII-D tokamak in San Diego and the Joint European Torus (JET) in Culham, are unable to produce higher electron temperatures. But the plasma conditions that lead to high electron temperatures have not been part of main-line fusion research. The high electron temperatures in PLT, for example, were achieved by seeding the plasma with neon to increase Z_{eff} of the plasma, and thus to increase the plasma resistivity, while at the same time the peak electron density was lowered to $1 - 2 \times 10^{13}$ cm^{-3} (cf. Fig. 3). In addition, a 2.45 GHz lower-hybrid heating and current drive system was used to to add additional power to the electrons (cf. Figs. 1 and 2). None of these techniques are used any longer.

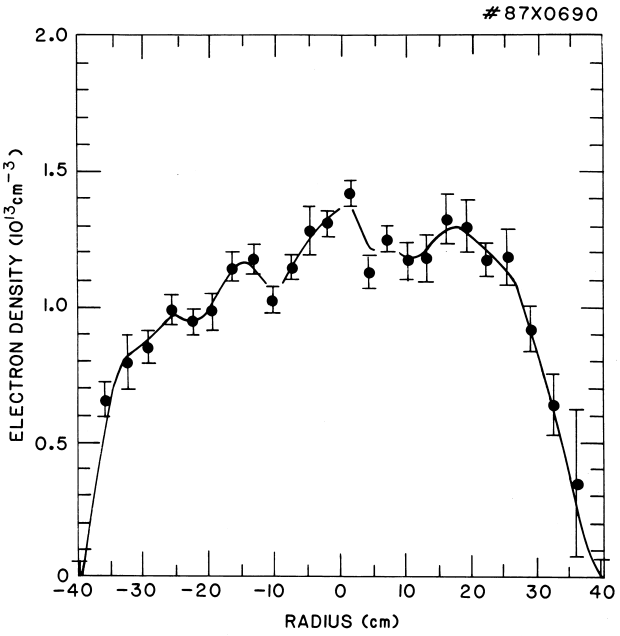

Figure 3. Radial electron density profile of typical PLT plasmas corresponding to discharges in Fig. 2.

ITER dwarfs all present-day tokamaks. Its plasma volume is more than a hundred times larger than that of PLT and almost ten times larger than that of JET. The electron temperature of ITER's plasma core is expected by design to achieve values of 20 – 30 keV during the high-performance discharges needed for fusion. A typical electron temperature profile predicted for one of the ITER performance scenarios is shown in Fig. 4. The corresponding predicted time histories of some of the ITER plasma parameters, including the presumed power input, are shown in Fig. 5. Note that ITER's electron density is assumed to be more than an order of magnitude higher than that in PLT.

The x-ray measurements on PLT [25] have established a scaling for the electron temperature required for a given neonlike ion to start producing measureable L-shell line radiation. Extrapolating this scaling from the observed neonlike Eu^{53+} to neonlike

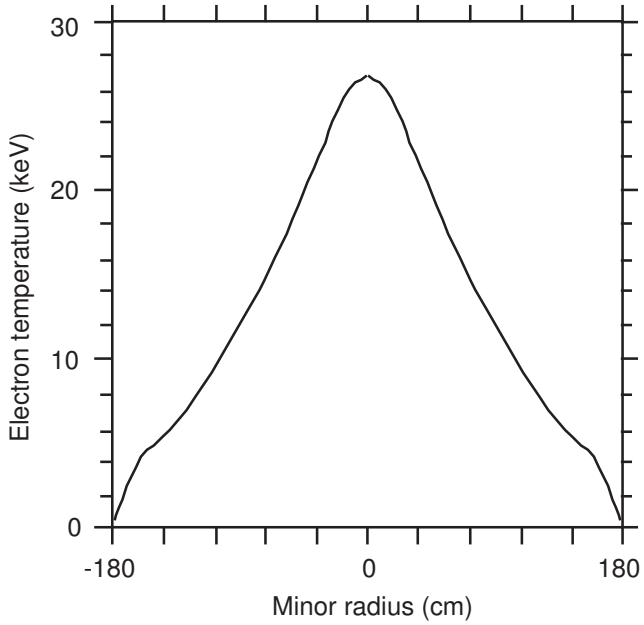

Figure 4. Predicted electron temperature profiles of high-performace ITER plasmas. Note the similarity in shape to the profiles shown in Fig. 2.

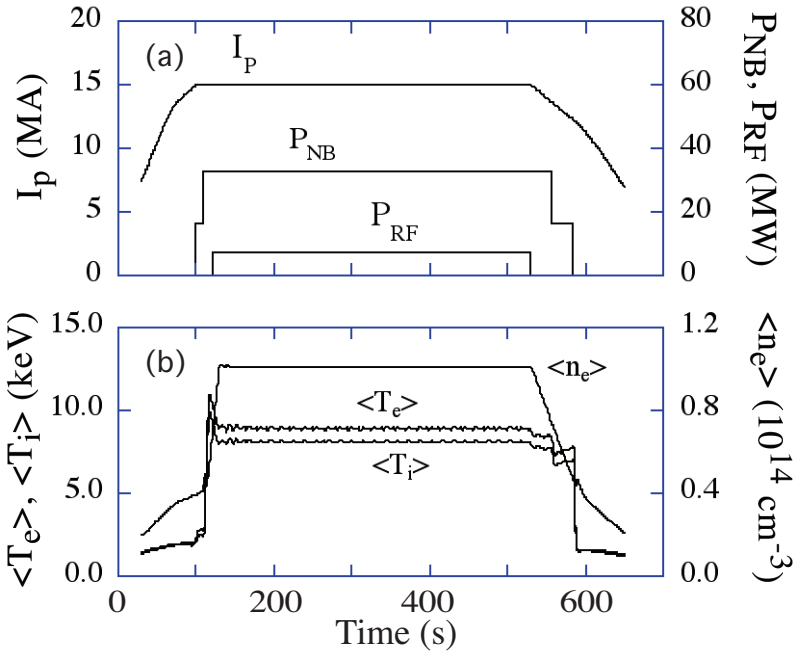

Figure 5. Time evolution of spatially averaged electron temperature ($\langle T_e \rangle$), ion temperature ($\langle T_i \rangle$), and electron density ($\langle n_e \rangle$), as well as plasma current (I_p) and heating power from neutral beam injection (P_{NB}) and radio-frequency wave injection (P_{RF}).

W^{64+} [23] gives a threshold electron temperature of 12 keV for producing measurable spectral lines. This agrees with ionization balance calculations using the Flexible Atomic Code (FAC) [26] presented in [23] and reproduced in Fig. 6. They show that W^{64+} has a fractional abundance of $\geq 5\%$ for temperatures between 10 and 35 keV. They also show that about 1% of tunsgten will be berylliumlike W^{70+} at 30 keV.

Noble gases, in particular argon, krypton, and xenon, are of interest to magnetic fusion research because they can be introduced via pellets and they can be pumped out without leaving residuals on plasma-facing components, i.e., they are not recycled in subsequent discharges. If krypton or xenon were injected into ITER, these noble gases would strip to heliumlike ions at the highest ITER temperatures. Indeed, early on it was proposed to inject krypton and use the K-shell emission of heliumlike Kr^{32+} [27] for diagnostics on ITER.

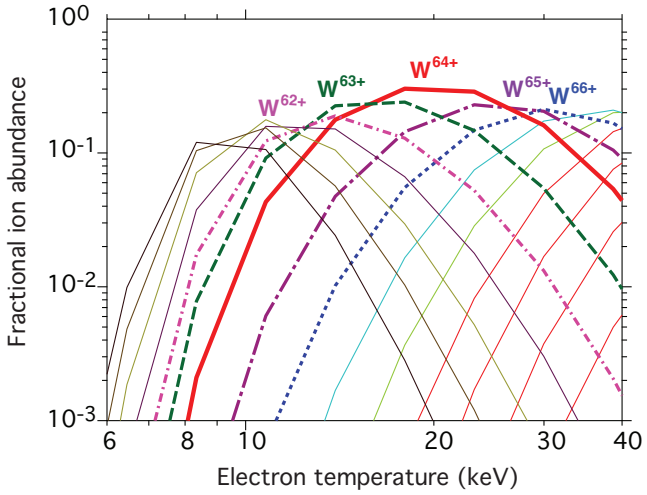

Figure 6. Predicted ionization balance of tungsten as a function of electron temperature showing the fractional ion abundances between W^{58+} and W^{72+}. [Adopted from [23].]

Initial ITER operation will be without high-power auxiliary heating, and, thus, the electron temperatures will likely be below 10 keV. Similar temperatures will be reached during the start-up phase of the discharge before auxiliary heating raises the temperature. In such "cold" plasmas, neither the tungsten L-shell lines nor the krypton K-shell lines can be used as a diagnostic. Even in high-power disharges with very high central electron temperatures, the colder regions $r/a \geq 0.5$ of ITER plasmas cannot be diagnosed with either neonlike tungsten or heliumlike krypton lines. Here r is the plasma minor radius, and a is its maximum value. Therefore, it has been proposed to diagnose the colder ITER plasmas by observing the K-shell emission from highly charged iron, in particular heliumlike Fe^{24+} or from hydrogenlike Fe^{25+} [23] (provided some plasma-facing components will be covered in stainless steel instead of beryllium, as now discussed [4]), or by observing the L-shell lines of neonlike xenon [28], provided

xenon will be injected for that purpose.

Argon is expected to be abundant in ITER plasmas and thus suggests itself for use in diagnosing "cold" ITER plasmas. Similarly, the M-shell line of near-nickellike tungsten ions or the L-shell lines of near-neonlike krypton could be used to diagnose the cooler plasmas. However, the line emission from all of these ions is below 4 keV and may thus not be energetic enough to penetrate the vacuum and tritium barriers that are an integral part of the CIXS [23]. Therefore, they may not play a role in high-resolution x-ray spectroscopy using the CIXS. However, these lines will likely be observed with the various survey-type instruments that monitor plasma performance near the plasma edge [29, 30, 31].

3. The Use of Highly Charged Ions for Plasma Diagnostics

Highly charged ions have been used for many diagnostic purposes in magnetic fusion research [32, 33]. In the following we will give examples of ion temperature and ion rotation measurements, electron temperature measurements, and ion diffusion experiments.

Although our examples focus on x-ray measurements, we point out that measurements in other wavelength bands can provide similar information. For example, the ion temperature and bulk ion motion can also be measured using lines in the ultraviolet [34, 35, 36], while measurements of charge exchange recombination with an energetic hydrogen neutral beam can be carried out with lines in the extreme ultraviolet region [37].

Lines from highly charged ions in the optical in many ways may be preferable to those in the vacuum ultraviolet, extreme ultraviolet, or x-ray regime. The reason being is that the use of lenses and light fiber optics together with the ready availability of very high resolution instrumentation greatly simplifies light gathering, shielding, spectral analysis, and recording. Several optical lines in highly charged tungsten ions have already been identified [38, 39, 40, 41]. However, the most abundant highly charged ions are those that assume a closed-shell or at least a closed-subshell electronic configuration, i.e., heliumlike, neonlike, argonlike, or nickellike. These ions typically emit photons preferentially in the x-ray regime.

Very high-resolution instrumentation is required to measure line profiles and line positions with very high accuracy. High-resolution x-ray spectroscopy has been a principal diagnostic of magnetic fusion plasmas since the first study of the broadening of the $1s2p\ ^1P_1 \rightarrow 1s^2\ ^1S_0$ resonance line in heliumlike Fe^{24+} by Bitter at al. [42] on PLT. Essentially all measurements have been accomplished by looking at the K-shell transitions of helium ions, such as Ar^{16+} [43, 44, 45, 46, 47], Ti^{20+} [48, 49], Cr^{22+} [50, 51], Fe^{24+} [52], and Ni^{26+} [53, 54]. The heliumlike ion with the highest atomic number so far measured spectroscopically on a tokamak is Kr^{34+} [55].

The CIXS [23] extends the legacy of high-resolution x-ray spectroscopy on tokamaks by using a spherically bent crystal to observe with high resolution lines from highly

charged ions in plasmas with temperature from about a few keV to about 30 keV. Very importantly, it will provide radial profiles of the x-ray emission of the plasma, as the instrument is based on an imaging scheme developed by Bitter *et al.* [56]. This scheme has now been successfully implemented on a variety of magnetic fusion devices since its initial use on the National Spherical Torus (NSTX) and Alcator C-mod [57, 58]. The CIXS will employ the lines of two or more of these five elements: argon, iron, krypton, xenon, and tungsten [23, 59]. The CIXS may be augmented with an x-ray microcalorimeter, which can also provide radial ion temperature measurements as well as monitor impurity ion content, however, with much lower time resolution [60].

3.1. Ion temperature and bulk ion motion measurements

Measurements of the ion temperature and ion velocity are both based on the Doppler effect, as illustrated in Fig. 7. The ion temperature is inferred from the Doppler broadening of a given line. In particular, the Doppler broadened line width $\Delta\lambda_{width}$ is related to the ion temperature T_i by the expression

$$\Delta\lambda_{width}/\lambda_0 = \sqrt{\frac{8\ln 2kT_i}{m_i c^2}}, \tag{1}$$

where m_i is the mass of the ion, λ_0 is the wavelength of the x-ray line at rest, k is the Boltzmann constant, and c is the speed of light.

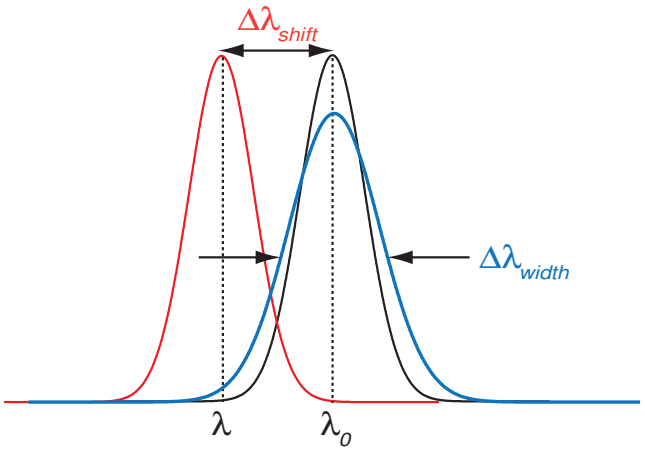

Figure 7. Principle of measuring the ion temperature and bulk ion motion using the Doppler effect. [Adopted from [6].]

The ion velocity is inferred from the Doppler shift $\Delta\lambda_{shift}$ of a given line. This shift is related to the bulk ion motion v_i by the expression

$$v_i = c\Delta\lambda_{shift}/\lambda_0. \tag{2}$$

The largest observable bulk plasma motion in a tokamak is the toroidal rotation. Thus, observations should be accomplished with a tangential viewing x-ray spectrometer. By

contrast, radially viewing instruments are used to measure the poloidal rotation, the magnitude of which is typically more than a factor of ten less than the toroidal rotation.

In order to make accurate measurements of line broadening or line shifts, it is necessary that the diagnostic line does not encounter blending by other lines, as such blending can lead to apparent line shifts and broadening unrelated to the Doppler effect. Such blending can occur by overlapping either with collisional or with dieletronic satellite lines. Blending with the latter is almost unavoidable, as shown early on in the case of K-shell spectra [61, 62], which means that these satellites must be very well characterized.

At an ion temperature of 30 keV, the broadening of the W^{64+} L-shell line is 9 eV, while the broadening of the Kr^{32+} K-shell line is 19 eV, i.e., twice as large. The broadening of an Fe^{24+} K-shell line at an ion temperature of 10 keV is about 7 eV, while that of Ar^{16+} is about 4 eV. Moreover, bulk toroidal velocities of 500 km/s may be possible in ITER. These shift a given line by similar amounts, e.g., the W^{64+} L-shell line shifts by about 10 eV. The maximum amount of broadening and shifting represents the wavelength space in which the diagnostic line should not encounter any other lines with which it could blend.

In addition to blending, there are instrumental line broadening and line shift effects that are systematically introduced by the Johann error. These effects cannot be avoided, even if the crystal is perfectly bent and focused. However, these effects are rather well understood, as discussed by Wang *et al.* [63]. In addition, a given line broadens because of its intrinsic line width given by the uncertainty principle. This so-called natural line width manifests itself especially at low ion temperatures, where it is no longer masked by a large Doppler broadening, as illustrated by Beiersdorfer *et al.* [64]. However, it must be taken into account at all ion temperatures in order to improve the accuracy of the ion temperature measurement.

An ITER requirement for the CIXS is that it be able to measure bulk ion velocities as low as 1 km/s. The Doppler shift of a given line must, therefore, be measured with great accuracy relative to some x-ray fiducial. Fluorescent x-ray lines from iridium or hafnium may provide such fiducials for the W^{64+} line [65]. In addition, the position of the x-ray line itself must be known with high accuracy.

3.2. Electron temperature measurements

Although measurements of the ion temperature and ion bulk velocities are often the prime reason for high-resolution spectroscopy, the measured x-ray spectra also provide the electron temperature. The reason is that most strong electric dipole allowed x-ray transitions are associated with satellite lines produced by dielectronic recombination. The intensity of the dielectronic satellite lines relative to the main x-ray line depends exponentially on the electron temperature, and, thus, it is a very sensitive diagnostic of electron temperature.

This ratio has been employed extensively in magnetic fusion plasmas to determine the electron temperature [66, 67, 68, 69]. The method was shown to work even in very

hot plasmas of the Tokamak Fusion Test Reactor (TFTR; $T_i = 20.7$ keV), in which the Doppler broadening nearly washed out the individual dielectronic satellites [70].

Electron temperature measurements have generally focussed on the dielectronic satellites to the dominant $1s2p\ ^1P_1 \rightarrow 1s^2$ K-shell line of heliumlike ions. In a few cases, the dielectronic satellites associated with the Lyman-α lines [71, 72, 73] or with the $1s3p\ ^1P_1 \rightarrow 1s^2\ ^1S_0$ transition [74, 75] were studied.

Electron temperature measurements are also possible using neonlike ions, albeit with reduced intensity of the dielectronic satellite [76]. This possibility is of importance for the planned operation of ITER and its focus on neonlike tungsten.

The strongest dielectronic satellite lines associated with the neonlike L-shell lines are produced by resonances involving a hole in the $2p$ sub-shell:

$$1s^2 2s^2 2p^6 + e^- \rightarrow 1s^2 2s^2 2p^5 n\ell n'\ell' \rightarrow 1s^2 2s^2 2p^6 n'\ell' + h\nu \tag{3}$$

The intensity of a given satllite line is given by the satellite line factor F_2 [77]:

$$F_2 = \frac{g_s}{g_i} \ \frac{A_a^{si} A_r^{sf}}{\Sigma_j A_a^{sj} + \Sigma_{f'} A_r^{sf'}}, \tag{4}$$

Here, A_a^{si} is the autoionization rate for decay of upper level $|s\rangle$ to the ground state $|i\rangle$ of the neonlike ion; A_r^{sf} is the rate of radiative decay of upper level $|s\rangle$ to lower level $|f\rangle$; g_s and g_i are the statistical weights of the autoionizing level and of the ground state of the target ion, respectively. The sum over f' extends over all levels lower than $|s\rangle$; the sum over $|j\rangle$ extends over all levels which are populated by autoionization of level $|s\rangle$.

The strongest dielectronic satellite lines are those that involve autoionizing states that have a large radiative decay rate A_r and a large autoionizing rate A_a with $A_r = A_a$. In this case F_2 achieves a maximum. For neonlike ions, the largest values of F_2 is obtained for $n, n' = 3$ and $\ell = n - 1 = d$. These are the satellites associated with the electric dipole allowed $3d \rightarrow 2p$ transitions in neonlike ions.

No tokamak measurements of dielectronic satellites of neonlike ions have been published so far. However, recently such satellite lines have been identified in the spectrum of neonlike iron observed on the star Capella [78, 79], as illustrated in Fig. 8. However, these measurements did not isolate dielectronic satellites of the type $n, n' = 3$ because these lines were also populated in a non-negligible way by electron-impact excitation [79]. Instead, the newly identified dielectronic satellite lines were of the type $n = 3$ and $n' = 4$. These lines cluster on the long-wavelength side closely to their neonlike parent line, and, very impartantly, they cannot be excited by any other mechanism in a coronal plasma.

In Fig. 9 we show the temperature dependence of the ratio of the intensity of the $n = 3$, $n' = 4$ dielectronic satellite line to the intensity of their neonlike Fe^{16+} parent line. The exponential dependence on the electron temperature is evident. This ratio was used to determine the coronal electron temperature of the star Capella [78], as indicated in the figure. This bodes well for identifying and utilizing dielectronic satellites of L-shell lines of neonlike ions on tokamaks in general, and of L-shell tungsten lines on ITER in

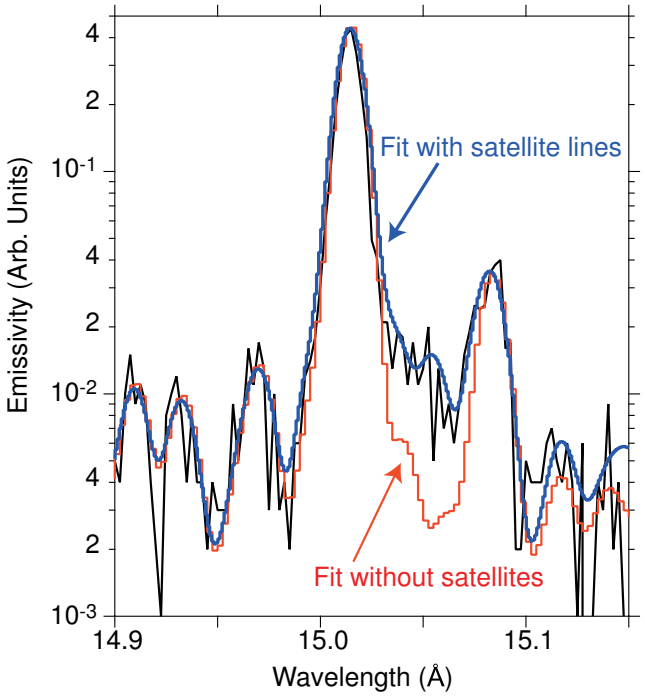

Figure 8. Spectrum of Capella produced by co-adding 298 ks of observations taking in the negative order with the high-energy grating. The observation is overlaid with a best fit model without (red line) and with including the $n = 3$, $n' = 4$ dielectronic satellite lines. [Figure adopted from [78].]

particular. However, their positions (including those that may blend with their parent line) and their intensities must be know accurately.

3.3. Transport measurements

Transport causes ions, and thus energy, to move across magnetic field lines. In general, transport in all magnetic confinement devices is larger than expected from theoretical considerations. As a result, transport measurements and, ultimately, control over transport are a major focal point of fusion research.

The radial flux Γ_q for charge states $+q$ is described by a model that includes diffusive and convective terms:

$$\Gamma_q = -D\frac{\partial n_q}{\partial r} + v_r n_q, \tag{5}$$

where D is the diffusion coefficient, v_r is the convective term, and n_q is the density of a given charge state. It is useful to use a semi-empirical parametrization of v_r and D. The radial velocity is typically [80] parametrized by introducing a parameter c_v and setting

$$v(r) = c_v D\frac{\partial \ln[n_e(r)]}{\partial r}. \tag{6}$$

D may be taken to be constant or to vary with r, time, and charge q of the ion.

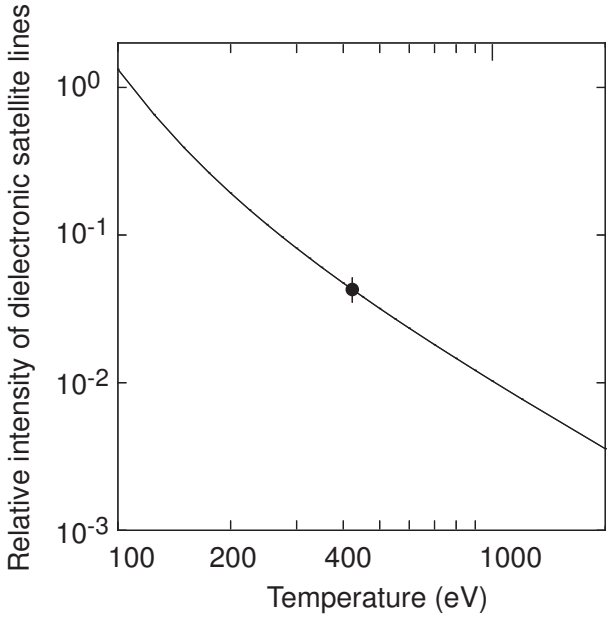

Figure 9. Calculated electron temperature dependence of the intensity of the $n = 3$, $n' = 4$ dielectronic satellite lines relative to the intensity of their $3d_{3/2} \rightarrow 2p_{1/2}\ ^1P_1$ parent line in neonlike Fe^{16+}. The point shown corresponds to measured intensities from observations of Capella's corona. [Figure adopted from [78].]

Spectra from highly charged ions can yield valuable transport information both when analyzing the time history of line intensities of injected heavy-element ions and when analyzing the radial profiles of the line intensities of intrinsic heavy-element ions in steady-state. In the following we briefly discuss both ways.

3.3.1. Time-dependent observations following heavy-element injection. Time dependent measurements of the line emission of highly charged ions have provided valuable insights into plasma transport and ion confinement [1, 81]. At first thought, it might appear that the time history of the intensity of an x-ray line of an element freshly injected into the plasma merely reflects the time it takes to ionize the element to the emitting ionization state. Modeling, however, shows that the time trace is also sensitive to the transport parameters D and c_v. In particular the initial rise of the intensity trace is strongly dependent on D, while the drop in the intensity after the peak value has been reached is sensitive to c_v (and to D).

We illustrate this in Figs. 10 and 11, where we show fits of the early and later times of the intensity of the $3d_{3/2} \rightarrow 2p_{1/2}$ transition in neonlike Se^{24+} produced after selenium was injected via laser blow-off into the plasma. The best fit is obtained by systematically varying the transport coefficients c_v and D, which are assumed to be constant along the plasma radius. The inferred values are $D = 5000$ cm^2/s and $c_v = 0$ [82].

The derived transport parameter values depend on the assumed ionization and

recombination coefficients, which determine how fast a given charge state is reached. High-quality ionization and recombination data are, therefore, crucial for accurate transport parameter measurements.

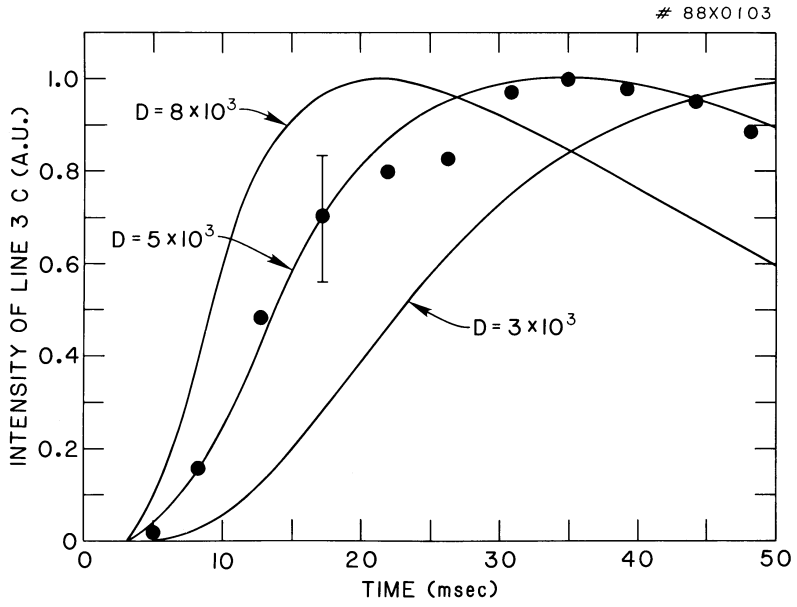

Figure 10. Measured and modeled intensity of the $3d \rightarrow 2p$ transition of neonlike Se^{24+}. The assumed values of D are shown in the figure. The value of c_v is set to zero. [Figure adopted from [82]].

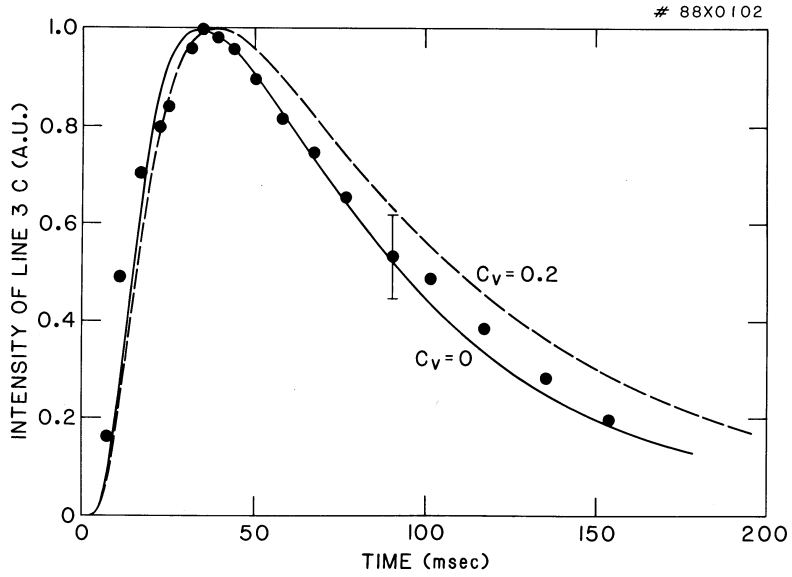

Figure 11. Time-dependent intensity of the $3d \rightarrow 2p$ transition of neonlike Se^{24+}. The data were modeled with $c_v = 0$ (dashed trace) and $c_v = 0.2$ (solid trace). The value of D is set to 5000 cm^{-2}. .

The mere observation that the overall signal decays in time after a peak is reached (cf. Fig. 11) is indicative of the fact that ion confinement in the plasma is finite. Once ionization equilibrium and spatial equilibrium are reached, the decay is exponential and proportional to the ion confinement time τ_p.

The exponential decay becomes clear when the time trace of the signal is plotted on a semi-logarithmic plot, as illustrated in Fig. 12. Here we compare the time evolution of the intensity of the $3d_{3/2} \rightarrow 2p_{1/2}$ transition in neonlike Se^{24+} recorded in plasmas heated either purely resistively (ohmically) by the plasma current or with additional heating using electromagnetic waves at the ion Bernstein wave (IBW) frequencies [83]. The exponential decay is twice as large in IBW-heated plasmas – 90 ms versus 45 ms in the ohmic plasma, although the electron density, electron temperature, and plasma current are the same for both plasmas. The lengthening of the decay time suggests an increase in the confinement time of the heavy ions, although the possibility of enhanced edge recycling of selenium during IBW heating cannot be ruled out.

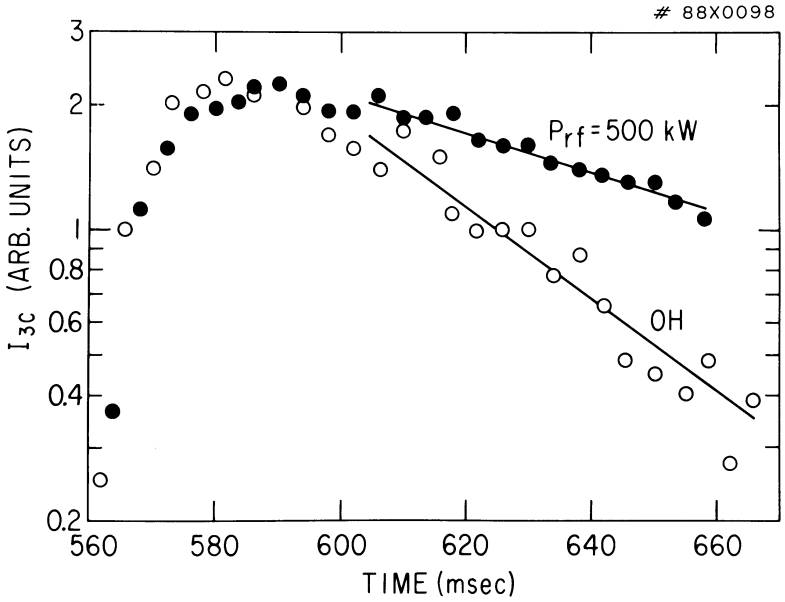

Figure 12. Time-dependent intensity of the $3d \rightarrow 2p$ transition of neonlike Se^{24+} during ohmically heated (OH) and ion-Bernstein wave heated plasmas. The power of the ion-Bernstein wave heating was $P_{rf} = 500$ kW. Selenium injection took place at $t = 560$ msec.

3.3.2. Steady-state observations of indigenous heavy-element ions. Despite their intrinsic utility, time-dependent measurements are not possible on many magnetic fusion devices, if only because of a lack of a suitable injector for the appropriate heavy element. Even in that case, it is still possbile to use the observed spectra for transport measurements, provided radial profiles of the line emission has been recorded.

Early on Bitter et al. noted that the K-shell emission spectrum of iron observed on a

tokamak differs from that expected in coronal equilibrium [84]. In part, this is because their measurements integrated along a line of sight through colder (edge) and hotter (center) parts of the plasma, which shifts the observed charge balance to lower charge states than expected from a uniform plasma set to a temperature equal to that of the core. (Setting the entire plasma temperature to the peak value may seem unreasonable at first; but calculations show that most of the radiation emanates from the hottest part of the plasma because of the exponential dependence of electron-impact excitation rates on the temperature.) But another reason is that ion transport changes the radial distribution of the ions in the plasma.

Finite values of the diffusion coefficient D results in ions of a given charge state migrating to colder or hotter plasma region than they would otherwise occupy otherwise. In other words, the spatial extent of a given ionization state broadens radially due to diffusion. This is illustrated in Fig. 13. For example, the radial abundance of neonlike Se^{24+} at the plasma center would be less than 0.25 at $r = 0$ for $D = 0$, but thanfraction increases to almost 0.8 for $D = 5000$ cm^{-2}, as illustrated in Fig. 13. Similarly, the radial profile of sodiumlike Se^{23+} broadens from about $r = 25$ cm to about $r = 30$ cm.

Measurements of the radial abundance profile of a given ionization state will elucidate the needed values of the transport parameters that produce the matching profile. For example, measured radial profiles of the line emission from sodiumlike Se^{23+}, neonlike Se^{24+}, and fluorineline Se^{25+} are shown in Fig. 14. These were obtained during the quasi steady-state decay phase after selenium injection discussed in the previous subsection. The ion abundance profiles *and* the relative ion abundance can be reproduced rather well using $D = 5000$ cm^2/s and $c_v = 0$ [82], but not with much larger or smaller values of D.

Determining transport parameters from such measurements requires accurate knowledge of the absolute and relative intensity of the primary diagnostic line and of the lines from the neighboring charge states, which in the case we illustrated means those of sodiumlike, neonlike, and fluorinelike selenium. It also requires that the ionization balance is known from a reliable ionization balance model. Of course, even in the absence of highly accurate atomic data, such measurements can be made, as we have shown. However, uncertainties in the atomic data translate in significant uncertainties in the inferred transport parameters.

4. Atomic data needs

In the following, we discuss the atomic physics issues associated with using x-ray lines for diagnosing magnetically confined plasmas in general and ITER plasmas in particular. For a given diagnostic line these include absolute wavelength determinations, in order to provide rest wavelength fiducials, and radiative transition rates, in order to deconvolve the line shapes. It also includes blending with dielectronic and innershell-excited satellite lines. We stress the need for excellent excitation and dielectronic recombination rates as well as for improved ionization balance calculations, as these are needed for extending

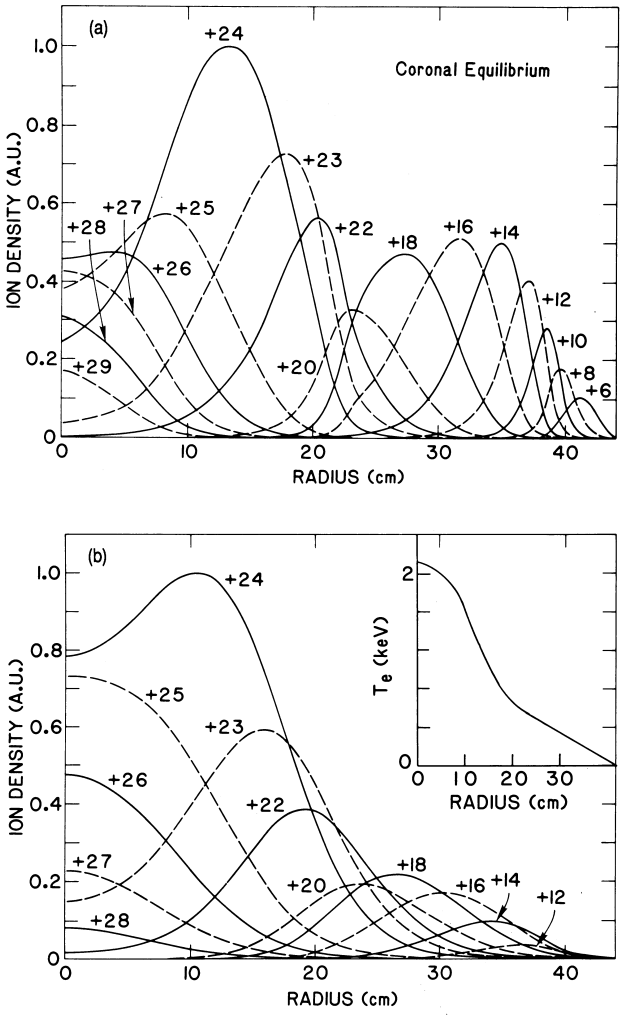

Figure 13. Predicted radial profiles of selenium ion abundances in the PLT tokamak. Two scalar radial diffusion coefficients were used: (a) D = 0 cm^2/s and (b) D = 5000 cm^2/s. The ion abundances were calculated using the electron temperature profile shown in the inset in (b) and assuming $c_v = 0$. [Adapted from [85].]

the utility of the CIXS to measure electron temperature and plasma transport.

The discussion of atomic data needs in the present section follows closely that presented at the 18th Conference on Atomic Processes in Plasmas held October 7–10, 2013, in Auburn, AL and summarized in the proceedings [59]. We repeat the discussion here in order to make it accessible to larger audience.

4.1. Required atomic parameters of the primary diagnostic line

4.1.1. Wavelengths. In many cases the rest wavelength if a given x-ray line is not known accurately enough to provide *absolute* bulk ion motion measurements on the order of 1 km/s. For example, the energy of the neonlike W^{64+} line has recently been measured to be 9126.25 ± 0.50 eV [86]. The experimental uncertainty is only sufficient

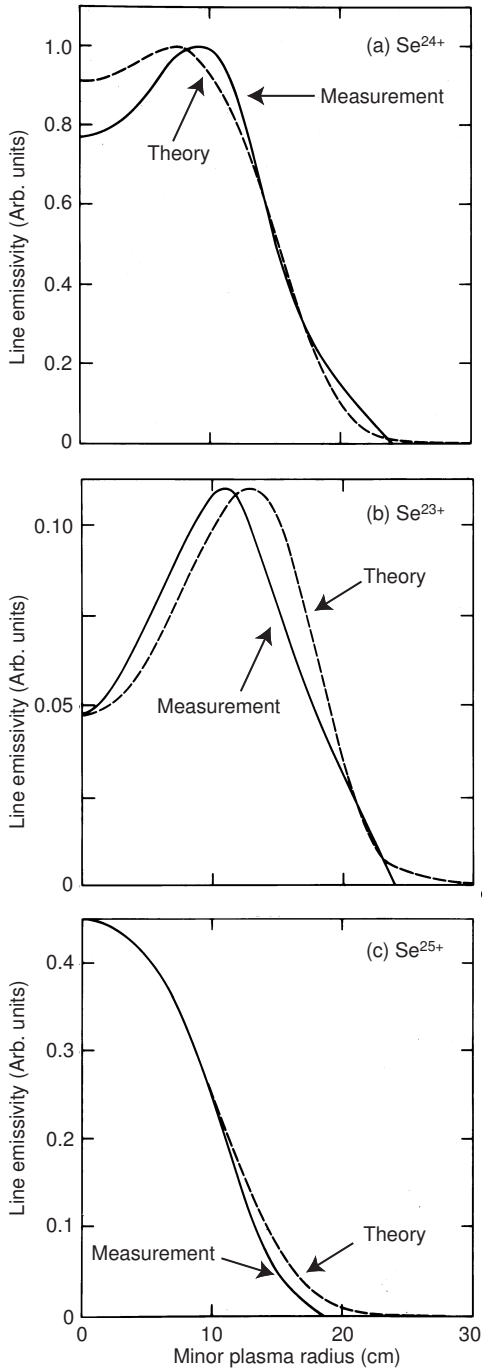

Figure 14. Measured (solid trace) and predicted (dashed trace) emissivity profiles of highly charged ions of selenium in the PLT tokamak: (a) neonlike Se^{24+}, (b) sodiumlike Se^{23+}, and (c) fluorinelike Se^{25+}. The calculations assume $D = 5000$ cm^2/s and $c_v = 0$. [Adapted from [82].]

to determine the absolute toroidal rotation velocity to within about 25 km/s. Thus, a measurement with 0.02 eV accuracy will be needed in the future. Similarly, the energy of the neonlike Xe^{44+} line has been measured to be 4557.74 ± 0.17 eV [25], while the energy

of the proposed heliumlike Kr^{32+} line has been measured to be $13114.68.14 \pm 0.36$ eV [87]. The heliumlike Fe^{24+} line was measured recently to be 6700.55 ± 0.07 [88], followed by a measurement of 6700.44 ± 0.07 [89]. Only the heliumlike Ar^{16+} line is known with sufficient experimental accuray to enable absolute measurements of line shifts associated with bulk ion velocities of 1 km/s. In particular, the energy of the Ar^{16+} line was measured to be 3139.583 ± 0.006 eV [90] and subsequently to be 3139.581 ± 0.005 eV [91]. The uncercertainyty of the latter value, however, has been revised upwards to 3139.581 ± 0.011 eV [89]. An overview of these measurements is given in Table 1.

Table 1. Overview of measured and calculated energies of various transitions under consideration for measurements with the CIXS.

Ion	Transition	$E_{Measured}$ (eV)	$E_{Calculated}$	$E_{Calculated}$
Ar^{16+}	$1s2p\ \ ^1P_1 \rightarrow 1s^2\ \ ^1S_0$	3139.583 ± 0.006^a	3139.58^b	3139.62^c
Fe^{24+}	$1s2p\ \ ^1P_1 \rightarrow 1s^2\ \ ^1S_0$	6700.55 ± 0.07^d	6700.40^b	6700.54^c
		6700.44 ± 0.07^e		
Kr^{34+}	$1s2p\ \ ^1P_1 \rightarrow 1s^2\ \ ^1S_0$	13114.68 ± 0.36^f	13144.33^b	13144.70^c
Xe^{44+}	$(1s^22s^22p^5_{3/2}3d_{5/2})_{J=1} \rightarrow (1s^22s^22p^6)_{J=0}$	4557.74 ± 0.17^g	4558.24^h	4559.38^i
W^{64+}	$(1s^22s^22p^5_{3/2}3d_{5/2})_{J=1} \rightarrow (1s^22s^22p^6)_{J=0}$	9126.25 ± 0.50^j	9125.28^h	9139.40^i

[a] Bruhns *et al.* [90]; [b] Drake [92]; [c] Cheng *et al.* [93];[d] Rudolph *et al.* [88]; [e] Kubicek *et al.* [89]; [f] Widmann *et al.* [87]; [g] Beiersdorfer *et al.* [86]; [h] Vilkas *et al.* [94]; [i] Ivanova and Gulov [95]; [j] Beiersdorfer *et al.* [86].

The theoretical wavelengths do not fare better than experimental wavelengths. Those for L-shell ions have generally insufficient accuracy to improve on the measured values. The comparison between measurements and calculations for the neonlike W^{64+} lines showed that even the calculations with the best agreement with experiment had an accuracy of only about 1 eV [86], which is still about twice the experimental accuracy. A comparison between measured and calculated values is given in Table 1.

The theoretical wavelengths for the K-shell lines of heliumlike and hydrogenlike ions are of much higher accuracy than those for the L-shell lines. In fact, these are often high enough to serve as reference lines for the measurement of the lines from ions with more electrons [96]. Tests of the calculations of the hydrogenlike lines have shown agreement within experimental error bars [96]. Tests of the calculations of the heliumlike lines have shown some systematic deviations between experiment and theory, although most measurements agree with theory within their respective experimental error bars [97]. These systematics have recently been attributed to uncalculated quantum electrodynamical terms [98], though that interpretation is highly controversial [99, 100]. As illustrated in Table 1, there are discrepancies between different calculations of the heliumlike transitions, and these are larger than desired for absolute velocity measurements.

We conclude that CIXS measurements of *absolute* bulk ion velocities need to rely on experimentally determined rest wavelengths. Highly accurate wavelength measurements of the L-shell lines and of the K-shell Kr lines are needed to fully make use of the diagnostic capabilities.

4.1.2. Radiative rates. The calculated radiative transition probabilities for the diagnostic lines of interest are around 1.1×10^{14} for argon [101] to 2.9×10^{15} s^{-1} for tungsten [95]. Such high rates can be measured by studying the lineshape in the (near) absence of Doppler broadening on electron beam ion traps, as originally demonstrated by Beiersdorfer *et al.* [64] for neonlike Cs^{45+}. These measurements showed that the calculations for neonlike x-ray lines are probably good to about 20%. For heliumlike systems the calculations achieved even better accuracy, probably better than a few percent, as recently demonstrated by Rudolph *et al.* [88] at a synchrotron facility.

A radiative rate of 2.9×10^{15} s^{-1} for the W^{64+} line corresponds by the uncertainty principle to a line width of about 1.84 eV. An error of 20 % corresponds to a line width uncertainty of 0.37 eV. This is a small value compared to the thermal broadening of the line. It will become only relevant if the ion temperature were very low ($\leq$ few keV). In that case the electron temprature would likely be very low as well, and the line emission would no longer be observable. The Ar^{16+} line can readily be produced at 1 keV, but its radiative rate is twenty times smaller than that for tungsten. Hence, even a 20% error in this rate gives a broadening uncertainty of only 0.014 eV, which has a negligible effect on ion temperature measurements. We conclude that the radiative rates of the primary diagnostic lines are known to sufficient accuracy, unless ITER's ion temperature is very low.

4.1.3. Excitation cross sections and rates. Excitation rates can typically be calculated with accuracies of 20% in the excitation cross sections. Photon rates estimated with the Flexible Atomic Code, for example, show that the proposed neonlike W^{64+} line emits 720 photons/ion/s at an electron temperature of 25 keV, while heliumlike Kr^{34+} emits only 90 photons/ion/s [23, 6]. Together with estimates of ion concentrations, crystal reflectivities, detector efficiencies, etc. it is then possible to estimate the signal rate and, thus, the smallest time interval that still produces sufficient signal for a meaningful measurement.

Absolute concentration measurements may require a higher accuracy of the excitation rates than is needed for making count rate estimates. The reason is that the measured line intensity must be unfolded with the excitation rate to extract the number of emitting ions. In addition, the instrumental response function must be known with equal confidence, requiring careful off-line calibration. Such a calibration may yield accuracies of better than 5%, which sets the requirement that excitation cross sections be known to within 5% or better in order to make absolute concentration measurements with such a level of accuracy.

Excitation rates also need to be known for *relative* concentration measurements,

i.e., for measurements of the abundance of the primary diagnostic ion species relative to the abundance of ions of neighboring charge states. Comparing these relative ratios to coronal ionization balance calculations will allow a determination of the transport coefficients, as discussed above. The required (relative) instrumental response is easier to characterize than the absolute response efficiency needed to make absolute concentration measurements. The accuracy of the excitation rates used to extract the relative concentrations, thus, still will need to be 5% or better in order to make best use of the available data.

Finally, excitation rates need to be known for electron temperature determinations. Such determinations use the relative intensity of the primary diagnostic line and its dielectronic satellite lines, as discussed in the previous Section. Thus, the technique requires not only accurate knowledge of the dielectronic satellite lines but also of the excitation rate of the parent line. It is imperative to know the excitation rates with very high accuracy, at least commensurate with the accuracy with which the dielectronic satellites are known or commensurate with the statistical quality with which the dielectronic satellites can be measured, which can vary between 1% and 10%, depending on the measurement scenario.

We note that the cross sections for electron-impact collisions, from which the required excitation rates are derived, have been only sparsely tested, and such tests have been exclusively performed on electron beam ion traps [102]. Measurements exist for the electron-impact cross section for exciting the K-shell lines of heliumlike iron and the heliumlike ions of neighboring elements [103, 104]. These show that cross section calculations are reliable to within about 10%. Cross section measurements of neonlike Fe^{16+} ions have shown discrepancies with theory on the order of 20% [105], while measurements of neonlike Ba^{46+} have shown agreement within the 15% error bars of the experiment [106]. No cross section measurements exist for either highly charged xenon or tungsten ions. Measurements of near-nickellike gold ions (gold has an atomic number that is five higher than tungsten), however, have shown discrepancies with calculations on the order of 50% [107].

4.1.4. Rates for indirect line excitation processes. We note that excitation by direct collisional impact is not the only process that contributes to the excitation rates of a given line. Indirect processes, such as cascade contributions, resonance excitation, innershell ionization of the lower ion species, radiative electron capture and dielectronic recombination by the higher ion species, and possibly charge exchange must also be considered [70, 108, 109, 110, 111, 112, 113]. Indirect processes and their rate coefficients must be folded into the rates for direct electron-impact excitation to produce an accurate line formation rate, in order to improve the diagnostic capabilities of the CIXS to measure absolute impurity concentrations, relative ion abundances for tranport parameter determinations, and electron temperatures. Although indirect processes represent typically only a small contribution to the overall excitation rate, they need to be known sufficiently well so that the overall excitation cross sections of the primary

diagnostic lines used by the CIXS maintains an accuracy of about 5% or better.

4.2. Required atomic parameters of collisional satellite lines

Collisional satellite lines are the lines from neighboring charge states that accompany the primary diagnostic line. In the case of heliumlike ions, these come foremost from $2p \rightarrow 1s$ transitions of lithiumlike, berylliumlike, and boronlike ions [87, 114, 115, 116, 117]. These collisional satellite lines all are situated on the low-energy side of the dominant heliumlike line. In the case of neonlike ions, these come foremost from $3d \rightarrow 2p$ transitions of sodiumlike, magnesiumlike, and aluminumlike ions on the low-energy side, and from $3d \rightarrow 2p$ transitions of fluorinelike and oxygenlike ions on the high-energy side [24, 25, 82, 86, 118]. The Lyman α lines of hydrogenlike ions do not have collisional satellites.

The required atomic parameters are essentially the same as those for the primary line, because these lines may serve as secondary diagnostics for T_i or v_i measurements, especially in plasma regions where the temperature is either higher or lower than needed to produce the maximum abundance of the charge state emitting the primary diagnostic line. In other words, it is necessary to know their positions and excitation rates with the same high accuracy as those associated with the primary diagnostic line. We note that collisional satellite lines associated with lower charge states generally emanate from autoionizing levels. This means that it is necessary to also know the branching ratios with the same accuracy as that of the excitation rates, because the product of the two determines the photon emission rate.

Knowledge of the spectral positions of collisional satellites is very important, as they may blend with the primary diagnostic. Such a blend would make the apparent position of the diagnostic line, and thus the apparent bulk ion velocity, dependent on the ionization balance. Similarly, a blend could broaden the diagnostic line. The positions of the collisional satellite lines have been measured for all of the proposed heliumlike diagnostics, and there is no possibility of line blends with the primary heliumlike diagnostic line [55, 87, 114, 119]. The collisional satellite lines of neonlike W^{64+} have been measured recently, and no interference with the primary diagnostic line was found [86].

4.3. Required atomic parameters of dielectronic satellite lines

The dielectronic recombination process starts with the same ion as the one that emits the primary diagnostic line. Thus, the ratio of the intensity of the dielectronic satellites and of the primary diagnostic line is independent of the assumed ionization equilibrium. It is simply a function of the dielectronic recombination resonance strength, of the excitation rate of the primary diagnostic line, and of the temperature.

Dielectronic satellite lines come in two basic flavors: Those that are fully resolved from the primary diagnostic line and typically are strong, and those that blend with the primary diagnostic line and are typically weak. But because of their sheer number

the weak lines may add considerable flux, as we have illustrated above in the case of neonlike Fe^{16+} (cf. Fig. 8).

In heliumlike spectra, the strong, well resolved dielectronic satellites are of the type $1s2p2\ell \rightarrow 1s^2 2\ell$ [120, 121]. As an example of such dielectronic satellites, we show in Fig. 15 the $1s2p2\ell \rightarrow 1s^2 2\ell$ dielectronic satellite lines of the K-shell spectrum of Kr^{34+}, which was measured on the Livermore electron beam ion trap [122].

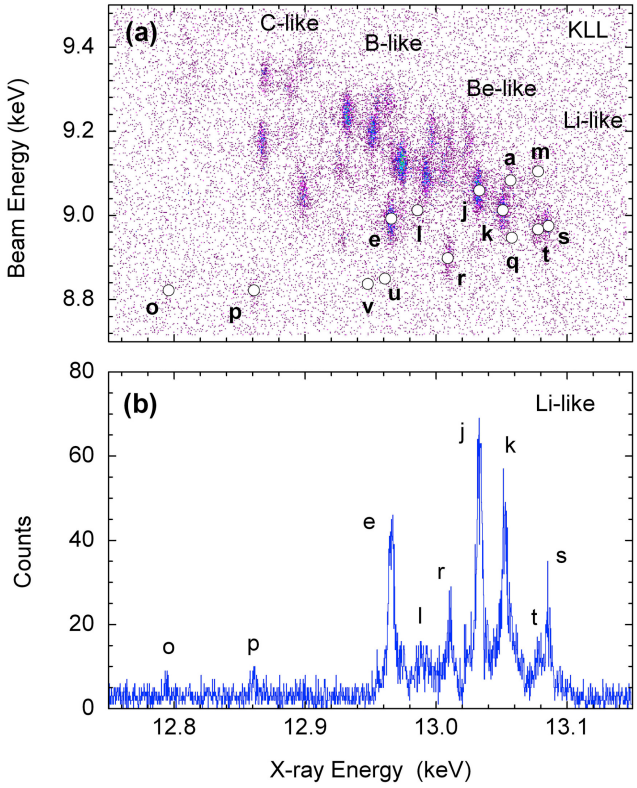

Figure 15. Dielectronic satellite contributions to the K-shell spectrum of Kr^{34+}. (a) Excitation function showing the resonant nature of the dielectronic recombination lines as a function of electron energy. (b) Spectrum of the dielectronic satellites associated with the $1s2p2\ell \rightarrow 1s^2 2\ell$ transitions in Kr^{33+}. The spectrum was generated by making a diagonal cut of the data presented in (a) and projecting the counts from lithiumlike lines onto the energy axis. The satellites are labeled using the standard notation of Gabriel [123]. The measurements were performed on the electron beam ion trap at Livermore.

The weaker satellite lines that blend with the primary heliumlike line are of the type $1s2pn\ell \rightarrow 1s^2 n\ell$ with $n \geq 3$ [61, 62, 124]. It is easy to see that as the principal quantum number n of the so-called spectator electron gets large, the dielectronic satellite lines become indistinguishable [125] from the heliumlike $1s2p \rightarrow 1s^2$ parent line, yet they need to be taken into account, as they induce a (small) shift in the centroid of the blended feature and change its intensity. This is illustrated in Fig. 16, where we show measurements of the high-n dielectronic satellites of Fe^{24+} made at the Livermore electron beam ion trap [70, 62].

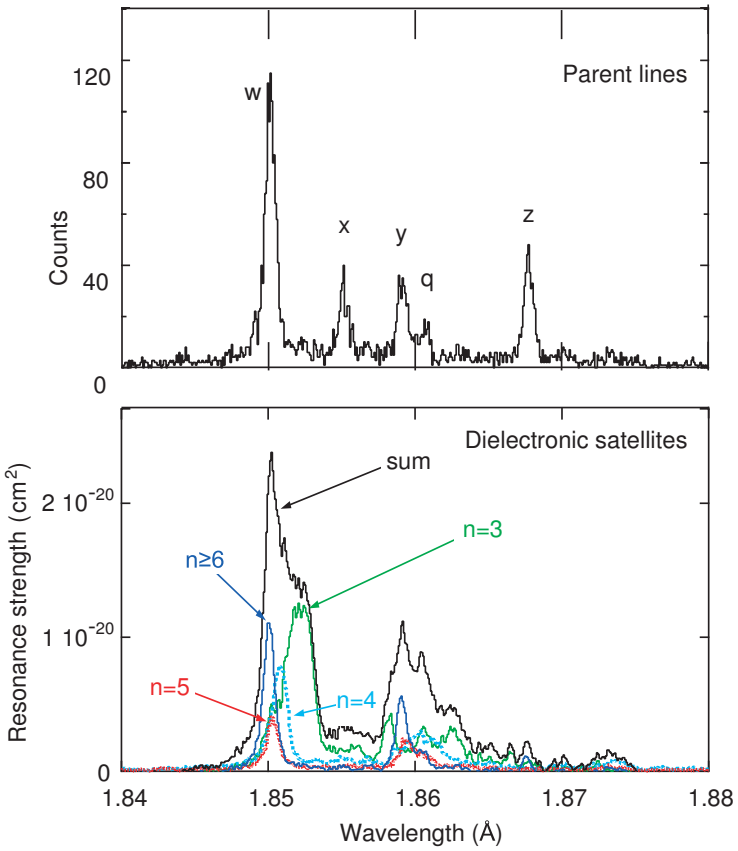

Figure 16. Dielectronic satellite contributions to the K-shell spectrum of Fe^{24+}. (a) Spectrum of the Fe^{24+} lines formed by collisional excitation, showing also one collisional satellite from Fe^{23+}, labeled q. (b) Spectra of the $n = 2 \rightarrow n = 1$ dielectronic satellites involving a spectator electron with principal quantum number $n = 3$ (green trace), $n = 4$ (light blue trace), $n = 5$ (red trace), $n \geq 6$ (dark blue trace), and the sum of these contributions (black trace). The measurements were performed on the electron beam ion trap at Livermore.

Both flavors of dielectronic satellite lines also occur in the x-ray spectra of neonlike ions. However, the intensity of the L-shell dielectronic satellites is greatly reduced compared to those found in the heliumlike spectra [76]. Recent measurements of the dielectronic satellite lines of neonlike Fe^{16+} performed on the Livermore electron beam ion trap [126] show that the $3d \rightarrow 2p$ transitions come with copious amounts of high-n ($n \geq 4$) dielectronic satellite lines that blend with their parent line. These measurements are shown in Fig. 18.

We note that all collisional satellite lines, as discussed in the previous section, that emanate from an autoionizing upper level can also be excited by dielectronic recombination, as dielectronic capture is the inverse process of autoionization. Typically, this contribution is relatively small, but it must be separately determined for each line used as a plasma diagnostic.

Dielectronic satellites have been measured with high accuracy in the spectra of

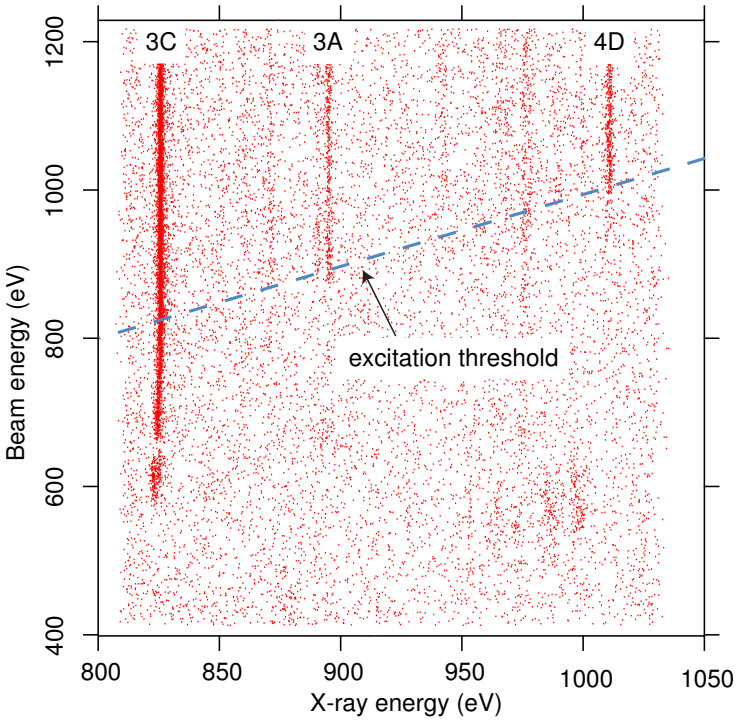

Figure 17. Excitation function as a function of electron energy of several Fe^{16+} lines (above threshold for electron-impact excitation) and the associated high-n ($n \geq 4$) dielectronic recombination satellite lines (below). The lines labeled $3C$, $3A$, and $4D$ emanate from upper levels $(2s^2 2p^5_{1/2} 3d_{3/2})_{J=1}$, $(2s_{1/2} 2p^6 3p_{3/2})_{J=1}$, and $(2s^2 2p^5_{3/2} 4d_{5/2})_{J=1}$, respectively. All three transitions terminate in the $(2s^2 2p^6)_{J=0}$ ground level. The measurements were performed on the electron beam ion trap at Livermore.

heliumlike ions [53, 54, 66, 127], and the temperatures inferred from the ratio of these lines to the heliumlike diagnostic line have agreed very well with those obtained on tokamaks from Thomson scattering. In fact, even the heavily broadened lines of Fe^{24+} in TFTR plasmas with $T_i = 20.7$keV and $T_e = 8.2$ keV could be used to extract T_e with high accuracy [70], as we already mentioned earlier. Moreover, an analysis of the K-shell emission line spectrum of heliumlike argon showed excellent agreement between models and observation from NSTX plasmas, indicating that dielectronic satellite spectra are very well understood theoretically and experimentally [119]. In addition, the dielectronic satellite strengths of heliumlike ions have been studied on electron beam ion traps [120, 62, 128, 129, 130, 131, 132, 133, 134, 135], and these measurements have displayed very good agreement (20% or better) between calculation and measurement for the strongest (or spectrally integrated) satellites; somewhat poorer agreement (disagreements larger than 20%) has been found for the spectrally resolved satellites, especially for some of the weaker lines.

We are not aware of high-resolution spectroscopic measurements, apart from the recent measurements on the Livermore electron beam ion trap [126] mentioned

above. Only recently have such lines been identified in the high-resolution spectrum of neonlike Fe^{16+} obtained in coronal plasmas [78] followed by an analysis of the spectrum of fluorinelike Fe^{17+} [136]. Integral measurements of the total contributions of these satellites to the associated dielectronic recombination rates, however, have been performed for both neonlike xenon and neonlike gold, and good agreement with theory was found within the roughly 15% error limits [137, 138].

Calculations have recently been carried out using many body perturbation theory atomic structure codes to assess the strengths and positions of the dielectronic satellite lines in the L-shell spectrum of W^{64+} [139, 140]. These calculations may guide future experimental investigations. Research identifying and measuring the high-n dielectronic satellite lines in neonlike ions is definitely needed to improve the reliability of L-shell diagnostic lines. This includes measuring both the position and strength of the dielectronic satellite lines associated with the primary diagnostic line. We stress that high spectral resolution will be needed in order to accurately locate the satellite lines.

Measurements of the dielectronic satellites associated with the collisional satellite lines will also be useful, as those lines may also be used for determining ITER plasma parameters. Moreover, dielectronic recombination is one of the 'indirect' line formation processes mentioned in Section 4.1.4, which links a higher charge state to the intensity of a primary diagnostic lines. As a consequence, understanding the contribution dielectronic recombination makes in populating the diagnostic L-shell lines will also be useful to calculate and measure.

4.4. Accurate knowledge of the ionization balance

Reliable extraction of the transport parameters depends on the quality of the calculated ionization balance. Ionization balance and ion transport codes, such as the multiple ion species transport (MIST) computer code [80] or the atomic data and analysis structure (ADAS) code [141], have in the past used rather crude atomic physics. This crudeness was the result of the lack of accurate ionization and recombination rates at the time, and in many instances multipliers for ionization and recombination rates had to be used to match the observed data [142]. An overview of the need for accurate ionization balance calculations, including those for tungsten, was recently been given by Beiersdorfer *et al.* [143]. Despite these short-comings in the ionization balance calculations such transport codes could be used to extract meaningful transport coefficients, as we have illustrated in the previous section, albeit without being able to specify stringent uncertainty limits on the inferred transport parameters.

Refinements of the underlying rates can lead to significant changes in the ion abundances as a function of the electron temperature, as demonstrated over the years in the well studied case of iron [144, 145, 146, 147]. Moreover, the rates involved in ionization balance calculations depend on the electron density. The coronal approximation, which assumes that all ionization and recombination proceeds from the ground state of a given ion, is violated even in the relatively low-density plasmas found in

magnetically confined plasma devices. For example, heliumlike and neonlike ions have metastable levels well above the ground state that have a non-negligible population fraction because they are forbidden to decay by electric-dipole allowed transitions, and neighboring charge states typically have a non-negligible mixing of the ground state population among the fine-structure levels [114, 148, 149].

A series of code comparison workshops on improving ionization balance models have shown remarkable progress in getting different computer codes to generate more reliable answers [150, 151, 152, 153, 154]. In part this was driven by the recent availability of measured ionization balances of high-Z ions, notably gold [155, 156, 157, 158]; in part better agreement arose from the realization that most of the discrepancy derived from the way dielectronic recombination was treated. The latter was clearly demonstrated by May *et al.*, who showed that even resonances involving spectator electrons with n=14–17 make a large difference in such "simple" plasmas as those produced by an electron beam in an ion trap whose electron distribution function spreads a mere 50 eV [159]. This sensitive dependence of the ionization balance calculations on how the atomic processes involving autoionizing levels are treated means that such calculations need to be greatly expanded to include a very, very large number of levels that up to now have been ignored. Thus, even in the absence of ion transport, state-of-the-art ionization balance models used today suffer from inadequacies.

Continued research of dielectronic satellite lines has revealed that this is not the only resonant recombination process that must be included in ionization balance calculations. In particular, trielectronic recombination must be included as well. Dielectronic recombination involves two electrons – one free electron being captured, and one bound electron being promoted to a higher energy state. Trielectronic recombination involves three electrons – one free electron being captured, and two bound electrons being promoted to a higher energy state. A process involving the correlated excitation of two bound electrons appears unlikely and, thus, negligible. However, Beilmann et al. recently showed that this process whas a rate comparable or higher than dielectronic recombination for certain ions [160, 161]. So far, none of the ionization balance calculations have included any of these resonant recombination processes that involve more than two electrons. We discuss this further in Section 5.4.

While the inclusion of all recombination and excitation-autoionization channels in the ionization balance models is not yet possible for arbitrary high-Z ion species, especially those involving a partially open M-shell or N-shell, it may be possible to include these processes in models tailored specifically for the ions of interest to a given diagnsotic, such as the CIXS. Such models require accurate atomic data only for charge states near a closed K-shell, i.e., one-, two-, three-, four- and five-electron systems, or near a closed L-shell, i.e., eight-, nine-, ten-, eleven-, twelve-, and thirteen-electron ions so that the number of ionization states is greatly reduced. Moreover, the atomic structure is simplified, and the code comparison workshops have shown that most ionization balance calculations do a much better job near such closed shells than arbitrary open M-shell or open N-shell systems [143].

Improved ionization balance calculation of the CIXS-relevant ion species look tractable as a goal in the coming decade while ITER is being built. In fact, such limited ionization balance calculations could already be applied toward the analysis of data from present-day core imaging x-ray spectrometers, e.g., those measuring the x-ray spectrum of argon [58, 162].

5. Atomic physics studies of highly charged ions in magnetic fusion devices

By achieving electron temperatures above 1 keV and operating at densities close to that of solar flares, tokamaks have been the first plasma devices to produce the highly charged ions found in the solar corona. Moreover, the nearly coronal plasma density conditions in magnetically confined plasma devices allows for measurements with high spectral resolution. Unlike in laser-produced plasmas the spectral lines are not broadened by Stark effects, and because the ions are excited from the ground state or ground state fine structure levels the amount of spectral lines is greatly reduced. Unlike in beam-foil experiments, there is little Doppler motion to worry about as long as the plasma is viewed radially. As a consequence, tokamaks have been used early on to study a variety of highly charged ions for astrophysics and basic atomic physics, as well as for some more applied physics purposes [85]. For example, production of hydrogenlike Ar^{17+} enabled one of the first precison tests of the Lamb shift [163], and the observation of systematic differences between theory and tokamak measurements of the resonance lines in heliumlike ions [97] continues to generate controversy to this date [98, 99]. Tokamak measurements of La^{47+} x-ray lines were used to verify line coincidences for photo-pumped x-ray laser schemes [164], and measurements in the extreme ultraviolet provided reference standards for astrophysical iron L-shell lines [165], for test of QED in lithiumlike ions [166, 167, 168, 169], and to study spectra of highly charged ions of heavy elements [170, 171]. In the following we give a brief review of some of the past and present research with magnetically confined plasma devices.

5.1. Line identification in the spectra of highly charged heavy ions

Line identification has been a diagnostic necessity in fusion research in order to identify the impurities that are inadvertently released into the plasma as different heating scenarios are explored. Early work focused on the transition metals, such as titanium, chromium, iron, and nickel, as well as on noble gases that could be admixed to the plasma [172, 173, 174, 175, 176]. Once the possibility was created to inject any type of material into the plasma via laser injection [1], spectra of other metals were investigated [177, 178, 179].

In Fig. 18 we show the soft x-ray spectrum of highly charged gadolinium ions. The spectrum is dominated by transitions in nickellike Gd^{36+}, i.e., lines 6 and 39 in Fig. 18. A total of 54 peaks were reported [180]. Not all of these peaks have been identified. For example, peaks 44, 45, and 46 are unassigned even though these peaks are among the

strongest observed, which illustrates that there is much more work to do.

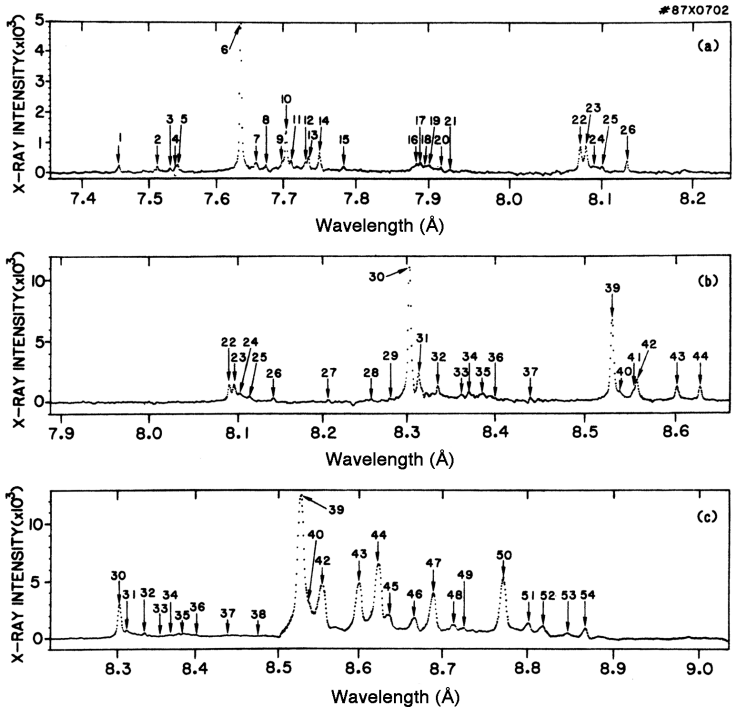

Figure 18. Spectra of highly charged gadolinium in the 7 to 9 Å region. Subfigures (a), (b), and (c) are from different discharges of the PLT tokamak.

Much of the spectroscopic research on highly charged ions has shifted in the meantime to electron beam ion traps, which are now widely available [181]. However, magnetic fusion devices still provide much needed spectroscopic data. For example, a very comprehensive study of the L-shell x-ray spectra of neonlike Kr^{24+}, Zr^{30+}, Nb^{31+} and Mo^{32+}, including collisional satellite lines, have been reported from the Alcator tokamak [182], and an analysis of the L-shell soft x-ray spectrum of neonlike Cu^{19+} was reported from NSTX [183]. In addition, the use of tungsten in plasma-facing components means that spectra of highly charged tungsten are being observed and studied [184, 185, 186].

5.2. Calibration of density-sensitive line ratios

Because magnetic fusion devices share the same electron density and temperature regime as solar flares they provide an ideal environment to test plasma kinetics and to perform laboratory x-ray astrophysics measurements [187]. In particular, they provide a test bed for calibrating astrophysically relevant density diagnostics [188, 189], as they can achieve densities several orders of magnitude higher than that afforded by electron beam ion traps.

We illustrate the calibration of density-sensitive line ratios in Fig. 19, where measurements of the intensity ratio of two density-sensitve siliconlike Fe^{12+} lines at

202.0 and 203.8 Å are plotted. This pair of lines, both of which are $3s^2 3p 3d \rightarrow 3s^2 3p^2$ transitions, is used as a density diagnostic for the solar transition region. Data from the Large Helical Device (LHD) [190] access the density region above 10^{13} cm^{-3} and provide data on the high-density limit of the ratio. Measurements from electron beam ion traps provide data between $5 \times 10^9 - 2 \times 10^{11}$ cm^{-3} [190, 191].

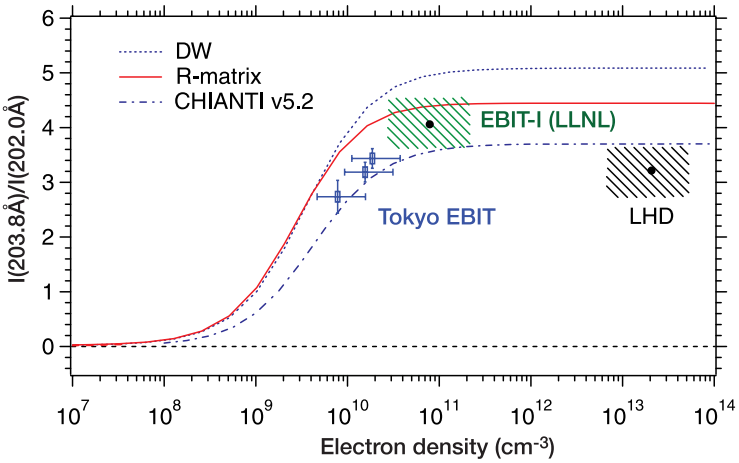

Figure 19. Electron density dependence of the intensity ratio of siliconlike Fe^{12+} lines at 202.0 and 203.8 Å. Measurements from the Livermore [190] and Tokyo [191] electron beam ion traps span the region between $5\times10^9-2\times10^{11}$ cm^{-3}. Data from the Large Helical Device [190] access the region above 10^{13} cm^{-3}. The three theoretical calculations shown are based on distorted-wave (DW) and R-matrix calculations as well as data from the CHIANTI atomic data base [192].

In Fig. 20 we show the density-sensitive ratio of the 114.4 and 117.2 Å line pair of boronlike Fe^{21+}. Both are $2s2p^2 \rightarrow 2s^2 2p$ transitions. The measured values are from the EBIT-I electron beam ion trap at Livermore, NSTX, and the Alcator C-Mod tokamak [189]. The experimental uncertainty of the EBIT-I data at low density is very high, and thus the testing of theory is not as good as desired. For comparison, we also show a measurement from the corona of the star Capella taken with the Chandra X-ray Observatory (for this datum the density is only assumed, not measured).

There are many astrophysically important density diagnostics based on spectral line pairs in highly charged ions. Clearly, more laboratory measurements will be needed to calibrate theoretical predictions. Magnetic fusion devices are best suited to do this in a systematic way because they calibrate the integrated atomic kinetics that enters density-sensitive line ratios in a Maxwell-Boltzmann plasma environment.

5.3. The Fe XVII problem

The soft x-ray L-shell emission from neonlike Fe^{16+} ions has been of great astrophysical interest, as the emission is observed from a wide variety of objects with both the Chandra and the XMM-Newton x-ray observatories [193]. The atomic physics underlying the line formation, however, has still not been fully described, as discussed in numerous papers

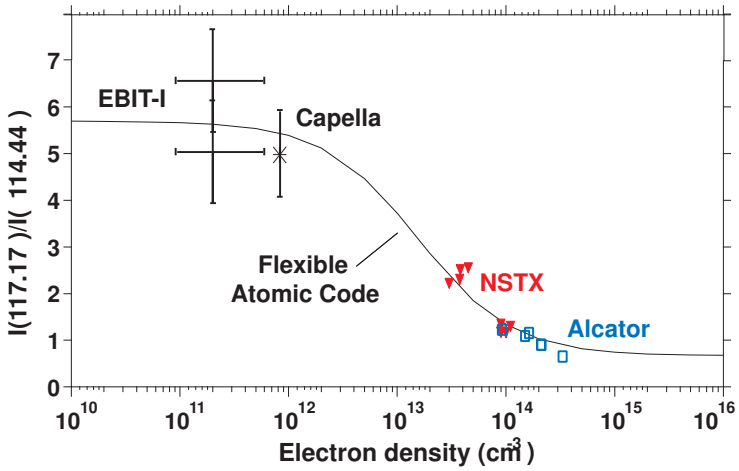

Figure 20. Electron density dependence of the intensity ratio of boronlike Fe^{21+} lines at 114.4 and 117.2 Å. Crosses are from the EBIT-I electron beam ion trap, the star is from satellite observations of the star Capella, filled triangles are from NSTX, and open squares are from the Alcator C-Mod tokamak. [Figure adapted from [189]].

[194, 195]. In other words, the intensity of these lines is not very well discribed by theory. The Fe XVII L-shell emission is, thus, like the calibration of density-sensitive line ratios another laboratory astrophysics problem.

Tokamaks measurements have been able to contribute to addressing the Fe XVII in multiple ways. Notably, because line formation processes in tokamaks are similar to those in stellar coronae, a direct comparison between the spectral emission from both types of plasmas can be made.

In Fig. 21 we show a spectrum of the soft x-ray emission in the 10 to 20 Å region that was recorded on NSTX using the X-ray and Extreme Ultraviolet Spectrometer (XEUS) [196, 197]. The five dominant L-shell transitions of Fe^{16+} situated in this region emanate from upper levels $(2s^2 2p^5_{1/2} 3d_{3/2})_{J=1}$ (labeled $3C$), $(2s^2 2p^5_{3/2} 3d_{5/2})_{J=1}$ ($3D$), $(2s^2 2p^5_{1/2} 3s_{1/2})_{J=1}$ ($3F$), $(2s^2 2p^5_{3/2} 3s_{1/2})_{J=1}$ ($3G$), and $(2s^2 2p^5_{3/2} 3s_{1/2})_{J=2}$ ($3H$, also often denoted $M2$). All five transitions terminate in the $(2s^2 2p^6)_{J=0}$ ground level.

The tokamak emission is optically thin in this wavelength region, so that the measured line ratios are unaffected by opacity effects. Interestingly, opacity effects in stellar coronae had been invoked to reconcile the observed solar line ratios with those from theory. However, the intensity ratios obtained in the tokamak measurements are essentially the same as those found in the Sun [198, 199], which ruled out opacity as the reason for the observed line ratios.

In Fig. 22 we illustrate the similarity of the L-shell Fe^{16+} line ratios inferred from astrophysical observations and tokamak measurements. By allowing an analysis of the various different line ratio, the tokamak measurements strongly suggest that spectral modeling predications have consistently overestimated the intensity of the dominant $3d \rightarrow 2p$ transition labeled $3C$ in Fig. 21 [198]. This is a point that experiments at electron beam ion trap and free-electron x-ray laser facilities are testing and confirming

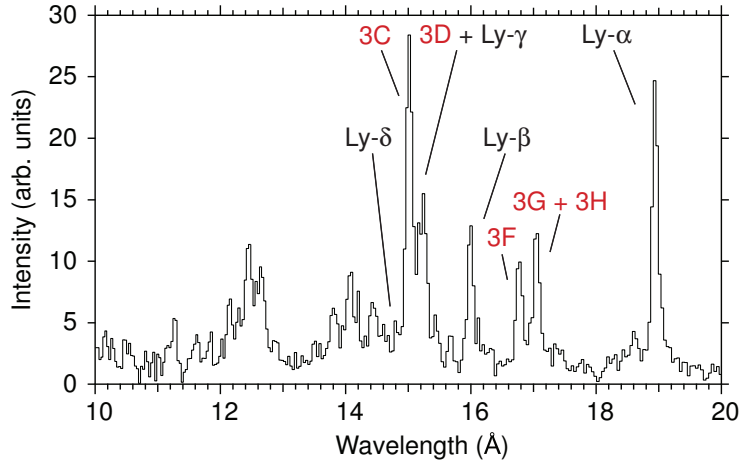

Figure 21. Soft x-ray emission between 10 and 20 Å recorded on NSTX. The L-shell emission lines from Fe^{16+} ions are labeled $3C$ through $3H$ in red; Lyman-series lines from hydrogenlike O^{7+} ions are labeled with Greek letters in black.Emission from higher charge states of iron produce the lines below 15 Å.

[105, 195].

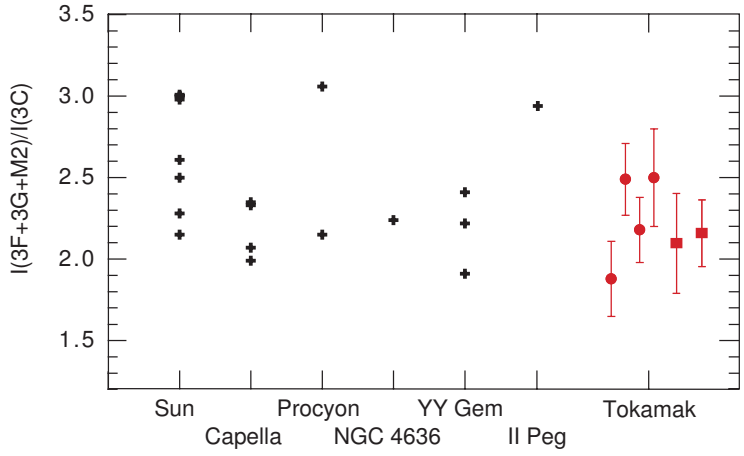

Figure 22. Comparison of tokamak $I_{3F+3G+M2}/I_{3C}$ ratios with those from solar and astrophysical measurements. The solar data are from [200, 201, 202, 203, 204]; stellar data are from [205, 206, 207, 208, 209, 210, 211]; the galactic datum is from [212]. Tokamak data are from [198].

Despite a large experimental and theoretical effort and much progress, the Fe XVII problem has not yet been satisfactorily solved. Measurements of the L-shell Fe^{16+} spectrum on tokamaks will, thus, continue to make important contributions.

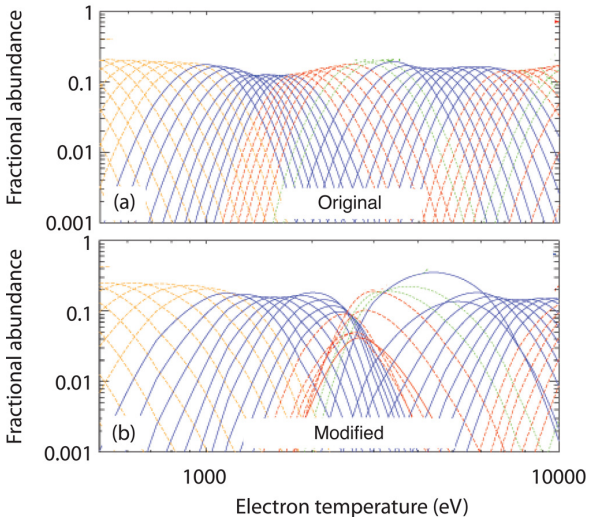

Figure 23. Fractional abundance of tungsten versus electron temperature at densities of 10^{14} cm^{-3}. (a) unmodified ADAS results, (b) using modified ionization and recombination rates to reproduce the ionization fractions seen in the ASDEX tokamak. [Figure adapted from [142].]

5.4. Testing ionization balance calculations

As we have stressed in the previous Sections, accurate ionization balance calculations are paramount to utilizing radial ion abundance profiles for inferring transport parameters. However, in cases where the transport parameters are known from other measurements, such as measurements employing a diagnostic neutral beam [213, 214], the problem can be inverted. Measurements of ion abundance profiles can then be used to hone the quality of the ionization balance calculations. As a result, magnetic fusion plasmas can be a sensitive test of ionization balance calculations.

A measurement of the ionization balance of tungsten in plasmas produced in the ASDEX Upgrade tokamak was recently obtained by Pütterich et al. [142]. The temperatures were typically below 4 keV, and the highest charge states were nickellike W^{46+} or slightly higher. The authors compared their measurements to the ionization balance predicted by the ADAS code [142], which is one of the ionization balance models used by the magnetic fusion community. The tungsten ionization fractions predicted by this code are shown in Fig. 23(a). In order to match their measurements, the authors needed to modify the ionization and recombination rates incorporated into ADAS. The resulting, semi-empirical ionization fractions are shown in Fig. 23(b). Evidently, the required modifications are substantial.

As illustrated by Fig. 23, well characterized magnetic fusion plasmas can provide benchmark data for the ionization fractions of heavy, highly charged ions. The tungsten ionization data from ASDEX Upgrade was compared to the results from a dozen ionization balance calculations performed by different teams and atomic physics codes for the 2013 code comparison workshop [215]. This comparison is shown in Fig. 24.

Although there is scatter among the results from the different calculations, all

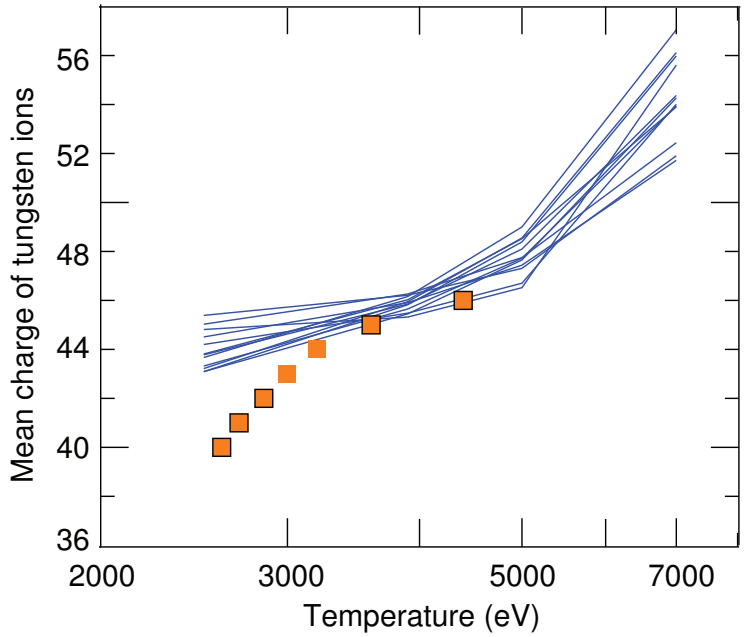

Figure 24. Mean charge of tungsten ions as a function of electron temperature: The solid blue lines are from different ionization balance calculations presented at the code comparison workshop NLTE-7 [from [215]]. Experimental data (orange squares) are from [142].

predictions lie consistenly above the experimental data. In other words, the mean charge of the tungsten ions is consistently predicted to be higher than actually measured on the ASDEX Upgrade tokamak. It also appears from the comparison in Fig. 24 that the discrepancy between calculations and measurements grows at the lower temperatures. At the lower temperatures the mean charge moves away from 46+, i.e. from the closed-shell nickellike ion configuration, and calculations are generally more uncertain [143, 215]. However, the systematic divergence between the calculations and measurements is striking.

In the previous Section we mentioned that trielectronic recombination may be as or more important than dielectronic recombination [160, 161], especially for ions away from closed shells. Such higher-order resonant recombination processes have not yet been included in *any* ionization balance calculation. Omitting these additonal recombination channels means that the mean ion charge will be predicted higher than it actually is. Although it is not yet clear how much of an effect trielectronic recombination has on the ionization balance of tungsten at the temperatures shown, we can infer from the divergence between calculations and measurements that the importance of trielectronic recombination is large (or that dielectronic recombination is not yet as adequately calculated as assumed) and increases as the mean ion charge tends towards ions with an open-shell electronic configuration.

5.5. Charge exchange

Astrophysical data have shown that charge exchange can produce x-ray emission from unexpected sources, such as comets, planetary atmospheres, and stellar winds [216, 217, 218]. X-ray production by charge exchange is, however, still only poorly described by spectral models, especially if charge exhange involves donor material that allows multi-electron capture [219, 220, 221]. By contrast, tokamak measurements enable the study of photon production by single electron capture and, thus, test the most basic photon production mechanisms.

In a tokamak environment charge exchange typically involves atomic hydrogen (or deuterium) as the neutral donor gas. It is provided by an energetic neutral beam that is purposefully injected into the plasma, or the hydrogen recycles from the wall and thus is cold (and may have recombined to form molecular hydrogen). The former interacts with highly charged ions in the hot core of the plasma, while the latter interacts with ions near the cooler edge of the plasma.

The first fine-structure resolved x-ray emission spectrum excited solely by charge exchange was recorded on the NSTX tokamak [111]. The spectrum was produced by hydrogenlike Ar^{17+} interacting with a 13–40 keV/amu deuterium neutral heating beam to produce heliumlike Ar^{16+}. While the $1s2p\ ^1P_1 \rightarrow 1s^2\ ^1S_0$ singlet transition produces the most intense line, denoted w, in collisional plasmas, it is no longer dominant in spectra produced by charge exchange, as illustrated in Fig. 25. The sum of the intensity of the three triplet lines is about four times that of the intensity of the singlet line.

The measured spectrum could be reproduced by a radiative cascade model, as shown in Fig. 25(b). The initial populations were determined based on charge exchange cross sections calculated by the classical trajectory Monte Carlo method [111]. The model yielded excellent agreement with the measurements, validating the modeling approach at high collision energies (> 10 keV/amu) in the case where only single electron capture is involved.

Interestingly, because hydrogen can exist for extended periods of time in the $2s$ exited state charge exchange may also populate levels otherwise inaccessible when hydrogen is in its ground state. About 0.5 % of the hydrogen in a neutral beam is in this metastable configuration [222]. Charge exchange with excited hydrogen is predicted to populate very high-lying levels. These levels may decay by x-ray emission, as first observed by Rice et al. [223]. Charge exchange with hydrogen in the $1s$ ground state is predicted to populate lower-lying levels, and their radiative decay can also be observed in the x-ray region [224, 225], Tokamak measurements can, thus, test predictions of charge exchange theory as to which Rydberg level is populated for interactions both with hydrogen in the $1s$ ground state and with hydrogen in the $2s$ excited state.

Charge exchange not only produces x-ray lines. As the Rydberg levels populated by the process radiatively decay, they produce lines in multiple wavelength bands. This can lead to the observation of unexpected lines, as, for example, the observation of lines from C^{4+} and C^{5+} reported recently from NSTX [226, 227].

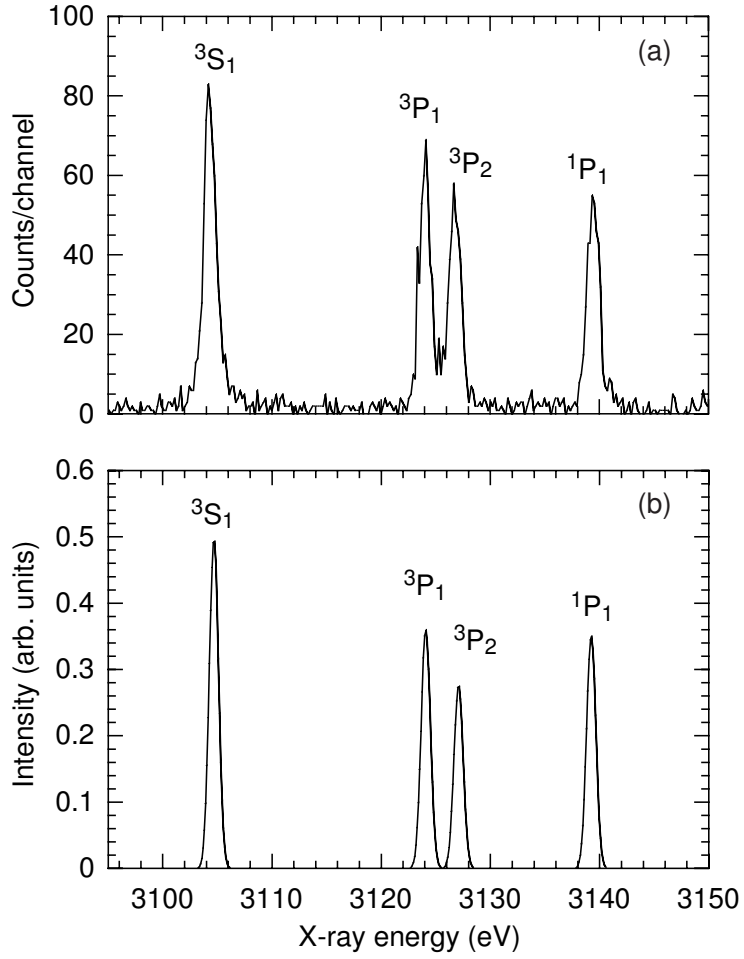

Figure 25. Spectrum of Ar^{16+} excited by charge exchange between Ar^{17+} ions and a 40 keV/amu neutral deuterium beam: (a) spectrum recorded on the NSTX tokamak; (b) model spectrum. The labels w, x, y and z denote the transitions from upper levels $1s2p\ ^1P_1$, $1s2p\ ^3P_2$, $1s2p\ ^3P_1$, and $1s2s\ ^3S_1$, respectively. [Adopted from [111].]

6. Conclusion

We have tried to show that studies of magnetic fusion plasmas consume a large amount of atomic data, especially in order to develop new and to improve existing the accuracy of spectral diagnostics. At the same time, these plasmas are excellent sources for producing atomic data of highly charged ions.

It should be kept in mind that magnetic fusion plasma are bright spectroscopic sources that easily can outshine electron beam ion traps. This means that uncertainties in spectra of highly charged ions obtained from magnetic fusion machines are typically not limited by photon statistics. ITER will have a huge volume and operate for about 400 s per discharge. Coupled with an electron temperature that will probably be above 10 keV even with moderate heating ITER plasmas can produce, for example, lithiumlike ions from high-Z elements for testing QED or effects of nuclear magnetism at levels of

accuracy that exceed those achieved on electron beam ion traps [228, 229, 230] or heavy-ion accelerators [231, 232]. Similarly, several current machines could provide such data – if the willingness existed to perform such basic science experiments.

Even at modest electron temperatures, magnetic fusion devices are capable of delivering data for astrophysically relevant highly charged ions. This includes calibrating density diagnostics, testing atomic kinetics, and investigating spectral formation by charge exchange. As we have shown, such work is in progress at various machines world-wide.

We have shown that the current focus on ITER and ITER-relevant plasmas requires data for essentially all charge states of tungsten. The high precision planned for the core imaging x-ray spectrometer requires are large set of atomic data of several highly charged ions from iron, krypton, xenon, and tungsten. Furthermore, data are needed to produce reliable ionization balance calculations as a prerequisite to develop or enhance transport diagnostics.

In brief, highly charged ions have played a prominent role in magnetic fusion plasmas in the past. They are an important component in current mangetic fusion research, and they will play a crucial role in the future, when fusion becomes a reality.

Acknowledgments

This work was performed under the auspices of the U. S. Department of Energy by Lawrence Livermore National Laboratory under Contract DE-AC52-07NA27344 and supported by the DOE Office of Fusion Energy Sciences. This work was carried out in part as a contribution to the International Atomic Energy Agency Coordinated Research Project "Spectroscopic and Collisional Data for Tungsten from 1 eV to 20 keV."

References

[1] Marmar E S, Cecchi J L and Cohen S A 1975 *Rev. Sci. Instrum.* **46** 1149
[2] Sudo S, Tamura N, Suzuki C, Muto S, Funaba H and the LHD Experiment Group 2012 *Nuclear Fusion* **52** 063012
[3] ITER Physics Expert Group on Divertor, ITER Physics Expert Group on Modelling and Database and ITER Physics Basic Editors 1999 *Nucl. Fus.* **39** 2391
[4] Lisgo S W, Börner P, Kukushkin A, Pitts R A, Polevoi A and Reiter D 2011 *Journal of Nuclear Materials* **415** 965
[5] Kramida A 2011 *Can. J. Phys.* **89** 551
[6] Clementson J, Beiersdorfer P and Lennartsson T 2013 *APPLICATION OF ACCELERATORS IN RESEARCH AND INDUSTRY: Twenty-Second International Conference* (*American Institute of Physics Conference Series* vol 1525) ed McDaniel F D, Doyle B L, Glass G A and Wang Y (New York: AIP) pp 78–83
[7] Suzuki C, Harte C S, Kilbane D, Kato T, Sakaue H A, Murakami I, Kato D, Sato K, Tamura N, Sudo S, Goto M, D'Arcy R, Sokell E and O'Sullivan G 2011 *Journal of Physics B Atomic Molecular Physics* **44** 175004
[8] Harte C S, Higashiguchi T, Otsuka T, D'Arcy R, Kilbane D and O'Sullivan G 2012 *Journal of Physics B Atomic Molecular Physics* **45** 205002

[9] Lennartsson T, Clementson J and Beiersdorfer P 2013 *Phys. Rev. A* **87** 062505

[10] Kilbane D, Gillaspy J D, Ralchenko Y, Reader J and O'Sullivan G 2013 *Physica Scripta Volume T* **156** 014012

[11] Safronova U I, Safronova A S and Beiersdorfer P 2011 *Canadian Journal of Physics* **89** 581–589

[12] Safronova U I, Safronova A S, Beiersdorfer P and Johnson W R 2011 Excitation energies, radiative and autoionization rates, dielectronic satellite lines and dielectronic recombination rates for excited states of Ag-like W from Pd-like W

[13] Safronova U I, Safronova A S and Beiersdorfer P 2012 *Phys. Rev. A* **86** 042510

[14] Safronova U I, Safronova A S and Beiersdorfer P 2012 *Journal of Physics B Atomic Molecular Physics* **45** 085001

[15] Aggarwal K M and Keenan F P 2014 *Atomic Data and Nuclear Data Tables* **100** 1603–1767

[16] Aggarwal K M and Keenan F P 2014 *Atomic Data and Nuclear Data Tables* **100** 1399–1518 (*Preprint* `1402.1126`)

[17] Aggarwal K M and Keenan F P 2014 *Canadian Journal of Physics* **92** 1166–1177 (*Preprint* `1401.4110`)

[18] Quinet P 2011 *Journal of Physics B Atomic Molecular Physics* **44** 195007

[19] Quinet P 2012 *Journal of Physics B Atomic Molecular Physics* **45** 025003

[20] Clementson J, Beiersdorfer P, Brage T and Gu M F 2014 *Atomic Data and Nuclear Data Tables* **100** 577–649

[21] Das T, Sharma L and Srivastava R 2012 *Phys. Scripta* **86** 035301

[22] Dipti, Das T, Sharma L and Srivastava R 2014 *Phys. Scripta* **89** 085403

[23] Beiersdorfer P, Clementson J, Dunn J, Gu M F, Morris K, Podpaly Y, Wang E, Bitter M, Feder R, Hill K W, Johnson D and Barnsley R 2010 *J. Phys. B* **43** 144008

[24] Beiersdorfer P, Bitter M, von Goeler S, Cohen S, Hill K W, Timberlake J, Walling R S, Chen M H, Hagelstein P L and Scofield J H 1986 *Phys. Rev. A* **34** 1297

[25] Beiersdorfer P, von Goeler S, Bitter M, Hinnov E, Bell R, Bernabei S, Felt J, Hill K W, Hulse R, Stevens J, Suckewer S, Timberlake J, Wouters A, Chen M H, Scofield J H, Dietrich D D, Gerassimenko M, Silver E, Walling R S and Hagelstein P L 1988 *Phys. Rev. A* **37** 4153

[26] Gu M F 2008 *Can. J. Phys.* **86** 191

[27] Barnsley R, O'Mullane M G, Ingesson L C and Malquias A 2004 *Rev. Sci. Instrum.* **75** 3743

[28] Beiersdorfer P, Lepson J K, Desai P, Díaz F and Ishikawa Y 2014 *Astrophys. J. (Suppl.)* **210** 16

[29] Seon C R, Choi S H, Cheon M S, Pak S, Lee H G, Biel W and Barnsley R 2010 *Review of Scientific Instruments* **81** 100000

[30] Seon C R, Hong J H, Jang J, Lee S H, Choe W, Lee H H, Cheon M S, Pak S, Lee H G, Biel W and Barnsley R 2014 *Review of Scientific Instruments* **85** 11E403

[31] Varshney S K, Barnsley R, O'Mullane M G and Jakhar S 2012 *Review of Scientific Instruments* **83** 10E126

[32] de Michelis C and Mattioli M 1981 *Nucl. Fus.* **21** 677

[33] Stratton B C, Bitter M, Hill K W, Hillis D L and Hogan J T 2008 *Fusion Sci. Techn.* **53** 431

[34] Suckewer S and Hinnov E 1977 *Nucl. Fus.* **17** 945

[35] Suckewer S and Hinnov E 1978 *Phys. Rev. Lett.* **41** 756

[36] Suckewer S, Eubank H P, Goldston R J, Hinnov E and Sauthoff N R 1979 *Phys. Rev. Lett.* **43** 207

[37] Skinner C, Suckewer S, Cohen S A, Schilling G, Wilson R and Stratton B 1984 *Phys. Rev. Lett.* **53** 458

[38] Utter S B, Beiersdorfer P and Brown G V 2000 *Phys. Rev. A* **61** 030503

[39] Watanabe H, Crosby D, Currell F, Fukami T, Kato D, Ohtani S, Silver J and Yamada C 2001 *Phys. Rev. A* **63** 042513

[40] Watanabe H, Nakamura N, Kato D, Sakaue H A and Ohtani S 2012 *Canadian Journal of Physics* **90** 497–501

[41] Kato D, Goto M, Morita S, Murakami I, Sakaue H A, Ding X B, Sudo S, Suzuki C, Tamura N,

Nakamura N, Watanabe H and Koike F 2013 *Physica Scripta Volume T* **156** 014081
[42] Bitter M, von Goeler S, Horton R, Goldman M, Hill K, Sauthoff N R and Stodiek W 1979 *Phys. Rev. Lett.* **42** 304
[43] Källne E, Källne J, Marmar E S and Rice J E 1985 *Phys. Scripta* **31** 551
[44] Lee S G, Bak J G, Nam U W, Moon M K, Shi Y, Bitter M and Hill K 2010 *Review of Scientific Instruments* **81** 10E506
[45] Shi Y, Wang F, Wan B, Bitter M, Lee S, Bak J, Hill K, Fu J, Li Y, Zhang W, Ti A and Ling B 2010 *Plasma Physics and Controlled Fusion* **52** 085014
[46] Pablant N A, Bitter M, Delgado-Aparicio L, Goto M, Hill K W, Lazerson S, Morita S, Roquemore A L, Gates D, Monticello D, Nielson H, Reiman A, Reinke M, Rice J E and Yamada H 2012 *Review of Scientific Instruments* **83** 083506
[47] Reinke M L, Podpaly Y A, Bitter M, Hutchinson I H, Rice J E, Delgado-Aparicio L, Gao C, Greenwald M, Hill K, Howard N T, Hubbard A, Hughes J W, Pablant N, White A E and Wolfe S M 2012 *Review of Scientific Instruments* **83** 113504
[48] Bitter M, Hill K W, Zarnstorff M, von Goeler S and Hulse R 1985 *Phys. Rev. A* **32** 3011–3029
[49] Lee P, Lieber A J and Wojtowicz S S 1985 *Phys. Rev. A* **31** 3996
[50] Platz P, Ramette J, Belin E, Bonnelle C and Gabriel A 1981 *J. Phys. E* **14** 448
[51] TFR Group, J Dubau, and M Loulergue 1982 *J. Phys. B* **15** 1007
[52] Bitter M, Hsuan H, Rice J E, Hill K W, Diesso M, Grek B, Hulse R, Johnson D W, Johnson L C and von Goeler S 1988 *Rev. Sci. Instrum.* **59** 2131
[53] Hsuan H, Bitter M, Hill K W, von Goeler S, Grek B, Johnson D, Bhalla C P, Karim K R, Bely-Dubau F and Faucher P 1987 *Phys. Rev. A* **35** 4280
[54] Bombarda F, Giannella R, Källne E, Tallents G J, Bely-Dubau F, Faucher P, Cornille M, Dubau J and Gabriel A H 1988 *Phys. Rev. A* **37** 504
[55] Bitter M, Hsuan H, Bush C, Cohen S, Cummings C J, Grek B, Hill K W, Schivell J, Zarnstorff M, Beiersdorfer P, Osterheld A, Smith A and Fraenkel B 1993 *Phys. Rev. Lett.* **71** 1007
[56] Bitter M, Hill K W, Roquemore A L, Beiersdorfer P, Kahn S M, Elliott S R and Fraenkel B 1999 *Rev. Sci. Instrum.* **70** 292
[57] Bitter M, Hill K W, Stratton B, Roquemore A L, Mastrovito D, Lee S G, Bak J G, Moon M K, Nam U W, Smith G, Rice J E, Beiersdorfer P and Fraenkel B S 2004 *Rev. Sci. Instrum.* **75** 3660
[58] Ince-Cushman A, Rice J E, Bitter M, Reinke M L, Hill K W, Gu M F, Eikenberry E, Broennimann C, Scott S, Podpaly Y, Lee S G and Marmar E S 2008 *Rev. Sci. Instrum.* **79** 10E302
[59] Beiersdorfer P, Clementson J, Widmann K, Bitter M, Hill K W, Johnson D, Barnsley R, Chung H K and Safronova U I 2015 *AIP Conference Proceedings* **in press** xxx
[60] Beiersdorfer P, Brown G V, Clementson J, Dunn J, Morris K, Wang E, Kelley R L, Kilbourne C A, Porter F S, Bitter M, Feder R, Hill K W, Johnson D and Barnsley R 2010 *Rev. Sci. Instrum.* **81** 10E323
[61] Bitter M, von Goeler S, Hill K W, Horton R, Johnson D, Roney W, Sauthoff N, Silver E and Stodiek W 1981 *Phys. Rev. Lett.* **47** 921
[62] Beiersdorfer P, Schneider M B, Bitter M and von Goeler S 1992 *Rev. Sci. Instrum.* **63** 5029
[63] Wang E, Beiersdorfer P, Gu M, Bitter M, Delgado-Aparicio L, Hill K W, Reinke M, Rice J E and Podpaly Y 2010 *Review of Scientific Instruments* **81** 10E329
[64] Beiersdorfer P, Osterheld A L, Decaux V and Widmann K 1996 *Phys. Rev. Lett.* **77** 5353
[65] Beiersdorfer P, Brown G V, Graf A T, Bitter M, Hill K W, Kelley R L, Kilbourne C A, Leutenegger M A and Porter F S 2012 *Rev. Sci. Instrum.* **83** 10E111
[66] Bitter M, Hill K W, Sauthoff N R, Efthimion P C, Merservey E, Roney W, von Goeler S, Horton R, Goldman M and Stodiek W 1979 *Phys. Rev. Lett.* **43** 129
[67] Faucher P, Loulergue M, Steenman-Clark L and Volonté S 1983 *Astron. Astrophys.* **118** 147
[68] M L Apicella, R Bartiromo, F Bombarda, and R Giannella 1983 *Phys. Letters* **98A** 174
[69] K-D Zastrow, E Källne, and H P Summers 1990 *Phys. Rev. A* **41** 1427

[70] Bitter M, Hill K W, von Goeler S, Stodiek W, Beiersdorfer P, Rice J E and Ince-Cushman A 2008 *Can. J. Phys.* **86** 291

[71] Decaux V, M Bitter and H H, Hill K W, von Goeler S, Park H and Bhalla C P 1991 *Phys. Rev. A* **44** R6987

[72] Decaux V, Bitter M, Hsuan H, von Goeler S, Hill K W, Hulse R A, Taylor G, Park H and Bhalla C P 1991 *Phys. Rev. A* **43** 228

[73] Rice J E, Reinke M L, Ashbourn J M A, Gao C, Victora M M, Chilenski M A, Delgado-Aparicio L, Howard N T, Hubbard A E, Hughes J W and Irby J H 2014 *Journal of Physics B Atomic Molecular Physics* **47** 075701

[74] Smith A J, Bitter M, Hsuan H, Hill K W, von Goeler S, Timberlake J, Beiersdorfer P and Osterheld A 1993 *Phys. Rev. A* **47** 3073

[75] Beiersdorfer P, Osterheld A L, Phillips T W, Bitter M, Hill K W and von Goeler S 1995 *Phys. Rev. E* **52** 1980

[76] P Beiersdorfer, PhD thesis, Princeton University 1988

[77] Dubau J and Volonté S 1980 *Rep. Prog. Phys.* **43** 199

[78] Beiersdorfer P, Gu M F, Lepson J and Desai P 2011 *16th Cambridge Workshop on Cool Stars, Stellar Systems, and the Sun* (*Astronomical Society of the Pacific Conference Series* vol 448) ed Johns-Krull C, Browning M K and West A A (San Francisco: Astronomical Society of the Pacific) p 787

[79] Beiersdorfer P, Bode M P, Díaz F and Ishikawa Y 2014 *Astrophys. J.* **793** 99

[80] Hulse R A 1983 *Nucl. Technol. Fusion* **3** 259

[81] TFR Group 1983 *Nucl. Fus.* **23** 559

[82] Beiersdorfer P, von Goeler S, Bitter M, Hill K W, Hulse R A and Walling R S 1989 *Rev. Sci. Instrum.* **60** 895

[83] M Ono, P Beiersdorfer, R Bell, S Bernabei, A Cavallo, A Chmyga, S Cohen, P Colestock, G Gammel, G J Greene, J Hosea, R Kaita, I Lehrman, G Mazzitelli, E Mazzucato, D McNeill, K Sato, J Stevens, J Timberlake, J R Wilson, and A Wouters 1988 *Phys. Rev. Lett.* **60** 294

[84] M Bitter, S von Goeler, N Sauthoff, K Hill, K Brau, D Eames, M Goldman, E Silver, and W Stodiek, in *International Conference on X-ray Processes and Inner-Shell Ionization, Stirling, Scotland, 1980* edited by D J Fabian, H Kleinpoppen, and L M Watson (Plenum Press, New York, 1981), p 861

[85] Beiersdorfer P, Bitter M, von Goeler S and Hill K W 1989 *Nucl. Instrum. Meth. B* **43** 347

[86] Beiersdorfer P, Lepson J K, Schneider M B and Bode M P 2012 *Phys. Rev. A* **86** 012509

[87] Widmann K, Beiersdorfer P, Decaux V and Bitter M 1996 *Phys. Rev. A* **53** 2200

[88] Rudolph J K, Bernitt S, Epp S W, Steinbrügge R, Beilmann C, Brown G V, Eberle S, Graf A, Harman Z, Hell N, Leutenegger M, Müller A, Schlage K, Wille H C, Yavaş H, Ullrich J and Crespo López-Urrutia J R 2013 *Physical Review Letters* **111** 103002

[89] Kubiček K, Mokler P H, Mäckel V, Ullrich J and Crespo López-Urrutia J R 2014 *Phys. Rev. A* **90** 032508

[90] Bruhns H, Braun J, Kubiček K, Crespo López-Urrutia J R and Ullrich J 2007 *Phys. Rev. Lett.* **99** 113001

[91] Kubiček K, Mokler P H, Ullrich J and Crespo López-Urrutia J R 2013 *Physica Scripta Volume T* **156** 014005

[92] G W F Drake 1988 *Can. J. Phys.* **66** 586

[93] Cheng K T, Chen M H, Johnson W R and Sapirstein J 1994 *Phys. Rev. A* **50** 247

[94] Vilkas M J, López-Encarnación J M and Ishikawa Y 2008 *At. Data Nucl. Data Tables* **94** 50

[95] E P Ivanova and A V Gulov 1991 *At. Data Nucl. Data Tables* **49** 1

[96] Beiersdorfer P 2009 *Can. J. Phys.* **87** 9

[97] Beiersdorfer P, Bitter M, von Goeler S and Hill K W 1989 *Phys. Rev. A* **40** 150

[98] Chantler C T, Kinnane M N, Gillaspy J D, Hudson L T, Payne A T, Smale L F, Henins A, Pomeroy J M, Tan J N, Kimpton J A, Takacs E and Makonyi K 2012 *Phys. Rev. Lett.* **109**(15)

153001
[99] Epp S W 2013 *Physical Review Letters* **110** 159301
[100] Beiersdorfer P and Brown G V 2015 *Phys. Rev. A* **in press** xxx
[101] Johnson W R, Savukov I M, Safronova U I and Dalgarno A 2002 *Astrophys. J. (Suppl.)* **141** 543
[102] Chen H and Beiersdorfer P 2008 *Can. J. Phys.* **86** 55
[103] S Chantrenne, P Beiersdorfer, R Cauble, and M B Schneider 1992 *Phys. Rev. Lett.* **69** 265
[104] Wong K L, Beiersdorfer P, Reed K J and Vogel D A 1995 *Phys. Rev. A* **51** 1214
[105] Brown G V, Beiersdorfer P, Chen H, Scofield J H, Boyce K R, Kelley R L, Kilbourne C A, Porter F S, Gu M F, Kahn S M and Szymkowiak A E 2006 *Phys. Rev. Lett.* **96** 253201
[106] R E Marrs and M A Levine and D A Knapp and J R Henderson 1988 *Phys. Rev. Lett.* **60** 1715
[107] May M J, Beiersdorfer P, Jordan N, Scofield J H, Reed K J, Hansen S B, Fournier K B, Gu M F, Brown G V, Porter F S, Kelley R, Kilbourne C A and Boyce K R 2005 *Nucl. Instrum. Methods* **B 235** 231
[108] Beiersdorfer P, Osterheld A L, Chen M H, Henderson J R, Knapp D A, Levine M A, Marrs R E, Reed K J, Schneider M B and Vogel D A 1990 *Phys. Rev. Lett.* **65** 1995
[109] Beiersdorfer P 1990 *in X-ray and Inner-Shell Processes, Knoxville, TN 1990, AIP Conference Proceedings No. 215, ed. by T. A. Carlson, M. O. Krause, and S. T. Manson (AIP, New York, 1990), p. 648*
[110] D A Vogel, P Beiersdorfer, R Marrs, K Wong, and R Zasadzinski 1991 *Z. Phys. D* **21** S193
[111] Beiersdorfer P, Bitter M, Marion M and Olson R E 2005 *Phys. Rev. A* **72** 032725
[112] Beiersdorfer P 2005 *X-ray Diagnostics of Astrophysical Plasmas: Theory, Experiment, and Observation* (*American Institute of Physics Conference Series* vol 774) ed Smith R (New York: AIP) pp 83–92
[113] Beiersdorfer P, Schweikhard L, Liebisch P and Brown G V 2008 *Astrophys. J.* **672** 726
[114] Beiersdorfer P, Phillips T, Jacobs V L, Hill K W, Bitter M, von Goeler S and Kahn S M 1993 *Astrophys. J.* **409** 846
[115] Tarbutt M R and Silver J D 2002 *J. Phys. B* **35** 1467
[116] Beiersdorfer P, Bitter M, Hey D and Reed K J 2002 *Phys. Rev. A* **66** 032504
[117] Thorn D B, Gu M F, Brown G V, Beiersdorfer P, Porter F S, Kilbourne C A and Kelley R L 2009 *Phys. Rev. Lett.* **103** 163001
[118] Källne E, Källne J and Cowan R D 1983 *Phys. Rev. A* **27** 2682
[119] Bitter M, Gu M F, Vainshtein L A, Beiersdorfer P, Bertschinger G, Marchuk O, Bell R, LeBlanc B, Hill K W, Johnson D and Roquemore L 2003 *Phys. Rev. Lett.* **91** 265001
[120] P Beiersdorfer, T W Phillips, K L Wong, R E Marrs, and D A Vogel 1992 *Phys. Rev. A* **46** 3812
[121] Biedermann C, Radtke R and Fournier K B 2002 *Phys. Rev. E* **55** 066404
[122] Widmann K, Beiersdorfer P, Decaux V, Elliott S R, Knapp D, Osterheld A, Bitter M and Smith A 1995 *Rev. Sci. Instrum.* **66** 761
[123] Gabriel A H 1972 *Mon. Not. R. Astron. Soc.* **160** 99
[124] P Beiersdorfer, M Bitter, M Chen, V Decaux, S Elliott, S Kahn, D Knapp, R Marrs, A Osterheld, D Vogel, and K Widmann, in *Atomic Processes in Plasmas*, ed by W L Rowan, AIP Conf Proc No 322 (American Institute of Physics, New York, 1995), p 129
[125] P Beiersdorfer, S Chantrenne, M H Chen, R Marrs, D Vogel, K Wong, and R Zasadzinski 1991 *Z. Phys. D* **21** S209
[126] Beiersdorfer P, Brown G V and Laska A 2015 *J. Phys. Conf. Ser.* **in press** xxx
[127] M Bitter, S von Goeler, S Cohen, K W Hill, S Sesnic, F Tenney, J Timberlake, U I Safronova, L A Vainshtein, J Dubau, M Loulergue, F Bely-Dubau, and L Steenman-Clark, Phys Rev A **29**, 661 (1984)
[128] D A Knapp, R E Marrs, M A Levine, C L Bennett, M H Chen, J R Henderson, M B Schneider, and J H Scofield 1989 *Phys. Rev. Lett.* **62** 2104
[129] Knapp D A, Marrs R E, Schneider M B, Chen M H, Levine M A and Lee P 1993 *Phys. Rev. A* **47** 2039

[130] Fuchs T, Biedermann C, Radtke R, Behar E and Doron R 1998 *Phys. Rev. A* **58**(6) 4518
[131] Smith A J, Beiersdorfer P, Widmann K, Chen M H and Scofield J H 2000 *Phys. Rev. A* **62** 052717
[132] Watanabe H, Currell F J, Kuramoto H, Li Y M, Ohtani S, O'Rourke B and Tong X M 2001 *J. Phys. B* **34** 5095
[133] Wargelin B J, Kahn S M and Beiersdorfer P 2001 *Phys. Rev. A* **63** 022710
[134] O'Rourke B E, Kuramoto H, Li Y M, Ohtani S, Tong X M, Watanabe H and Currell F J 2004 *Journal of Physics B: Atomic, Molecular and Optical Physics* **37** 2343
[135] Zhi-Min H, Jia-Min Y, Ji-Yan Z, Tuo Z, Bao-Han Z, Yao-Nan D, Zhi-Jian Z, Bin D, Yue-Ming L and Jun Y 2009 *Chinese Physics Letters* **26** 033401
[136] Clementson J and Beiersdorfer P 2013 *Astrophys. J.* **763** 54
[137] DeWitt D R, Schneider D, Chen M H, Clark M W, McDonald J W and Schneider M B 1992 *Phys. Rev. Lett.* **68** 1694
[138] Schneider M B, Knapp D A, Chen M H, Scofield J H, Beiersdorfer P, Bennett C, Henderson J R, Levine M A and Marrs R E 1992 *Phys. Rev. A* **45** R1291
[139] Safronova U I, Safronova A S and Beiersdorfer P 2009 *J. Phys. B* **42** 165010
[140] Safronova U I, Safronova A S and Beiersdorfer P 2009 *At. Data Nucl. Data Tables* **95** 751
[141] `http://adas.phys.strath.ac.uk`
[142] Pütterich T, Neu R, Dux R, Whiteford A D, OMullane M G and the ASDEX Upgrade Team 2008 *Plasma Phys. Control. Fusion* **50** 085016
[143] Beiersdorfer P, May M J, Scofield J H and Hansen S B 2012 *High Energy Dens. Phys.* **8** 271
[144] Arnaud M and Raymond J 1992 *Astrophys. J.* **398** 394
[145] Mazzotta P, Mazzitelli G, Colafrancesco S and Vittorio N 1998 *Astron. Astrophys. Suppl.* **133** 403
[146] Bryans P, Badnell N R, Gorczyca T W, Laming J M, Mitthumsiri W and Savin D W 2006 *Astrophys. J. (Suppl.)* **167** 343 (*Preprint* `arXiv:astro-ph/0604363`)
[147] Bryans P, Landi E and Savin D W 2009 *apj* **691** 1540
[148] Jacobs V L, Decaux V and Beiersdorfer P 1997 *J. Quant. Spectrosc. Rad. Transfer* **58** 645
[149] Beiersdorfer P, Obst M and Safronova U I 2011 *Phys. Rev. A* **83** 012514
[150] Lee R W, Nash K and Ralchenko Y 1997 *J. Quant. Spectrosc. Rad. Transfer* **58** 737
[151] Bowen C, Decoster A, Fontes C J, Fournier K B, Peyrusse O and Ralchenko Y V 2003 *J. Quant. Spectrosc. Rad. Transfer* **81** 71
[152] Rubiano J G, Florido R, Bowen C, Lee R W and Ralchenko Y 2007 *High Energy Dens. Phys.* **3** 225
[153] Fontes C J, Abdallah, Jr J, Bowen C, Lee R W and Ralchenko Y 2009 *High Energy Dens. Phys.* **5** 15
[154] Hansen S, Armstrong G S J, Bastiani-Ceccotti S, Bowen C, Chung H K, Colgan J P, de Dortan F, Fontes C J, Gilleron F, Marquès J R, Piron R, Peyrusse O, Poirier M, Ralchenko Y, Sasaki A, Stambulchik E and Thais F 2013 *High Energy Density Physics* **9** 523
[155] Foord M E, Glenzer S H, Thoe R S, Wong K L, Fournier K B, Wilson B G and Springer P T 2000 *Phys. Rev. Lett.* **85** 992
[156] Glenzer S H, Fournier K B, Wilson B G, Lee R W and Suter L J 2001 *Phys. Rev. Lett.* **87** 045002
[157] Wong K L, May M J, Beiersdorfer P, Fournier K B, Wilson B, Brown G V, Springer P, Neill P A and Harris C L 2003 *Phys. Rev. Lett.* **90** 235001
[158] Heeter R F, Hansen S B, Fournier K B, Foord M E, Froula D H, Mackinnon A J, May M J, Schneider M B and Young B 2007 *Phys. Rev. Lett.* **99** 195001
[159] May M J, Scofield J, Schneider M, Wong K, Beiersdorfer P and Hanson S B 2011 *Phys. Rev. E* **84** 046402
[160] Beilmann C, Mokler P H, Bernitt S, Keitel C H, Ullrich J, López-Urrutia J R C and Harman Z 2011 *Physical Review Letters* **107** 143201
[161] Beilmann C, Harman Z, Mokler P H, Bernitt S, Keitel C H, Ullrich J and Crespo López-Urrutia J R 2013 *Phys. Rev. A* **88** 062706

[162] Hill K W, Bitter M, Delgado-Aparicio L, Johnson D, Feder R, Beiersdorfer P, Dunn J, Morris K, Wang E, Reinke M, Podpaly Y, Rice J E, Barnsley R, O'Mullane M and Lee S G 2010 *Review of Scientific Instruments* **81** 10E322
[163] Marmar E S, Rice J E, Källne E, Källne J and LaVilla R E 1986 *Phys. Rev. A* **33** 774
[164] Beiersdorfer P, Nilsen J, Scofield J, Bitter M, von Goeler S and Hill K W 1995 *Phys. Scripta* **51** 322
[165] Sugar J and Rowan R L 1995 *J. Opt. Soc. Am. B* **12** 1403
[166] Denne B, Hinnov E, Ramette J and Saoutic B 1989 *Phys. Rev. A* **40** 1488
[167] Denne B, Magyar G and Jacquinot J 1989 *Phys. Rev. A* **40** 3702–3705
[168] Hinnov E, the TFTR Operating Team, Denne B and the JET Operating Team 1989 *Phys. Rev. A* **40** 4357
[169] Knize R J 1991 *Phys. Rev. A* **43** 1637–1639
[170] Hinnov E, Beiersdorfer P, Bell R, Stevens J, Suckewer S, von Goeler S, Wouters A, Dietrich D, Gerassimenko M and Silver E 1987 *Phys. Rev. A* **35** 4876
[171] Sugar J, Kaufman V and Rowan W L 1993 *Journal of the Optical Society of America B Optical Physics* **10** 1977–1979
[172] Hinnov E 1976 *Phys. Rev. A* **14** 1533–1541
[173] Hinnov E 1979 *Astrophys. J. (Lett.)* **230** L197–L199
[174] Hinnov E and Suckewer S 1980 *Physics Letters A* **79** 298–300
[175] Hinnov E, Suckewer S, Cohen S and Sato K 1982 *Phys. Rev. A* **25** 2293–2301
[176] Breton C, DeMichelis C, Hecq W, Mattioli M, Ramette J, Saoutic B, Bauche-Arnoult C, Bauche J and Wyart J F 1988 *Phys. Scripta* **37** 33–37
[177] Finkenthal M, Stratton B C, Moos H W, Hodge W L, Suckewer S, Cohen S, Mandelbaum P and Klapisch M 1985 *Journal of Physics B Atomic Molecular Physics* **18** 4393–4402
[178] Hinnov E, Boody F, Cohen S, Feldman U and Hosea J 1986 *Journal of the Optical Society of America B Optical Physics* **3** 1288–1294
[179] Jupén C, Denne-Hinnov B, Martinson I and Curtis L J 2003 *Phys. Scripta* **68** 230
[180] von Goeler S, Beiersdorfer P, Bitter M, Bell R, Hill K, LaSalle P, Ratzan L, Stevens J, Timberlake J, Maxon S and Scofield J 1988 *J. Phys. (Paris)* **49** C1_181
[181] Beiersdorfer P 2009 *Phys. Scripta* **T134** 014010
[182] Rice J E, Fournier K B, Goetz J A, Marmar E S and Terry J L 2000 *J. Phys. B* **33** 5435
[183] Safronova A S, Ouart N D, Lepson J K, Beiersdorfer P, Stratton B, Bitter M, Kantsyrev V L, Cox P G, Shlyaptseva V and Williamson K M 2010 *Review of Scientific Instruments* **81** 100000
[184] Chowdhuri M B, Morita S, Goto M, Nishimura H, Nagai K and Fujioka S 2008 *Plasma and Fusion Research* **2** 1060
[185] Clementson J, Beiersdorfer P, Magee E W, McLean H S and Wood R D 2010 *J. Phys. B* **43** 144009
[186] Podpaly Y A, Rice J E, Beiersdorfer P, Reinke M L, Clementson J and Barnard H S 2011 *Can. J. Phys.* **89** 591–597
[187] Beiersdorfer P 2003 *Ann. Rev. Astron. Astrophys.* **41** 343
[188] Beiersdorfer P, Brown G V, Kamp J B, Magee E W, Lepson J K, Podpaly Y and Reinke M L 2011 *Can. J. Phys.* **89** 653–656
[189] Lepson J, Beiersdorfer P, Gu M F, Desai P, Bitter M, Roquemore L and Reinke M L 2012 (*American Institute of Physics Conference Series* vol 1438) ed Aggarwal Dr K and Shearer Dr F (New York: AIP) pp 136–141
[190] Yamamoto N, Kato T, Funaba H, Sato K, Tamura N, Sudo S, Beiersdorfer P and Lepson J 2008 *Astrophys. J.* **689** 646
[191] Nakamura N, Watanabe E, Sakaue H A, Kato D, Murakami I, Yamamoto N, Hara H and Watanabe T 2011 *Astrophys. J.* **739** 17
[192] Dere K P, Landi E, Young P R, Del Zanna G, Landini M and Mason H E 2009 *Astron. Astrophys.* **498** 915–929

[193] Paerels F B S and Kahn S M 2003 *Ann. Rev. Astron. Astrophys.* **41** 291
[194] Brown G V 2008 *Can. J. Phys.* **86** 199
[195] Bernitt S, Brown G V, Rudolph J K, Steinbrügge R, Graf A, Leutenegger M, Epp S W, Eberle S, Kubiček K, Mäckel V, Simon M C, Träbert E, Magee E W, Beilmann C, Hell N, Schippers S, Müller A, Kahn S M, Surzhykov A, Harman Z, Keitel C H, Clementson J, Porter F S, Schlotter W, Turner J J, Ullrich J, Beiersdorfer P and Crespo López-Urrutia J R 2012 *Nature* **492** 225–228
[196] Beiersdorfer P, Bitter M, Roquemore L, Lepson J K and Gu M F 2006 *Rev. Sci. Instrum.* **77** 10F306
[197] Beiersdorfer P, Lepson J K, Bitter M, Hill K W and Roquemore L 2008 *Rev. Sci. Instrum.* **79** 10E318
[198] Beiersdorfer P, Bitter M, von Goeler S and Hill K W 2004 *Astrophys. J.* **610** 616
[199] Beiersdorfer P, von Goeler S, Bitter M and Thorn D B 2001 *Phys. Rev. A* **64** 032705
[200] Hutcheon R J, Pye J P and Evans K D 1976 *Mon. Not. R. Astron. Soc.* **175** 489
[201] Parkinson J H 1973 *Astron. Astrophys.* **24** 215
[202] McKenzie D L, Landecker P B, Broussard R M, Rugge H R, Young R M, Feldman U, and Doschek G A 1980 *Astrophys. J.* **241** 409
[203] Parkinson J H 1975 *Solar Phys.* **42** 183
[204] Rugge H R and McKenzie D L 1985 *Astrophys. J.* **297** 338
[205] Behar E, Cottam J and Kahn S M 2001 *Astrophys. J.* **548** 966
[206] Brinkman A C, Gunsing C J T, Kaastra J S, van der Meer R L J, Mewe R, Paerels F, Raassen A J J, van Rooijen J J, Bräuninger H, Burkert W, Burwitz V, Hartner G, Predehl P, Ness J U, Schmitt J H M M, Drake J J, Johnson O, Juda M, Kashyap V, Murray S S, Pease D, Ratzlaff P and Wargelin B J 2000 *Astrophys. J. (Lett.)* **530** L111
[207] Mewe R, a J J Raassen, Drake J J, Kaastra J S, van der Meer R L J and Porquet D 2001 *Astron. Astrophys.* **368** 888
[208] Canizares C R, Huenemoerder D P, Davis D S, Dewey D, Flanagan K A, Houck J, Markert T H, Marshall H L, Schattenburg M L, Schulz N S, Wise M, Drake J J and Brickhouse N S 2000 *Astrophys. J.* **539** L41
[209] Raassen A J J, Mewe R, Audard M, Güdel M, Behar E, Kaastra J S, van der Meer R L J, Foley C R and Ness J U 2002 *Astron. Astrophys.* **389** 228
[210] Stelzer B, Burwitz V, Audard M, Güdel M, Ness J U, Grosso N, Neuhäuser R, Schmitt J, Predehl P and Aschenbach B 2002 *Astron. Astrophys.* **392** 585
[211] Huenemoerder D P, Canizares C R and Schulz N S 2001 *Astrophys. J.* **559** 1135
[212] Xu H, Kahn S M, Peterson J R, Behar E, Paerels F B S, Mushotzky R F, Jernigan J G and Makishima K 2002 *Astrophys. J.* **579** 600
[213] Fonck R J and Hulse R A 1984 *Phys. Rev. Lett.* **52** 530
[214] Synakowski E J, Efthimion P C, Rewoldt G, Stratton B C, Tang W M, Grek B, Hill K W, Hulse R A, Johnson D W, Kissick M W, Mansfield D K, McCune D, Mikkelsen D R, Park H K, Ramsey A T, Redi M H, Scott S D, Taylor G, Timberlake J and Zarnstorff M C 1993 *Physics of Fluids B* **5** 2215–2228
[215] Chung H K, Bowen C, Fontes C J, Hansen S B and Ralchenko Y 2013 *High Energy Density Physics* **9** 645–652
[216] Cravens T E 2002 *Science* **296** 1042
[217] Wargelin B J and Drake J J 2002 *Astrophys. J.* **578** 503
[218] Bhardwaj A, Elsner R E, Gladstone G R, Cravens T E, Lisse C M, Dennerl K, Branduardi-Raymont G, Wargelin B J, Waite J H, Robertson I, Østgaard N, Beiersdorfer P, Snowden S L and Kharchenko V 2007 *Plan. Space Sci.* **55** 1135
[219] Beiersdorfer P, Boyce K R, Brown G V, Chen H, Kahn S M, Kelley R L, May M, Olson R E, Porter F S, Stahle C K and Tillotson W A 2003 *Science* **300** 1558
[220] Leutenegger M A, Beiersdorfer P, Brown G V, Kelley R L, Kilbourne C A and Porter F S 2010

Physical Review Letters **105** 063201 (*Preprint* 1008.2478)
[221] Ali R, Neill P A, Beiersdorfer P, Harris C L, Schultz D R and Stancil P C 2010 *apjl* **716** L95 (*Preprint* 1005.2599)
[222] Isler R C and Olson R E 1988 *Phys. Rev. A* **37** 3399
[223] Rice J E, Marmar E S, Terry J L, Källne E and Källne J 1986 *Phys. Rev. Lett.* **56** 50
[224] Wargelin B J, Beiersdorfer P, Liedahl D A, Kahn S M and von Goeler S 1998 *Astrophys. J.* **496** 1031
[225] Hedqvist A, O'Mullane M, Nordquist J, Rachlew-Källne E and Zastrow K D 2000 *Journal of Physics B Atomic Molecular Physics* **33** 375–382
[226] Lepson J K, Beiersdorfer P, Bitter M, Roquemore A L and Kaita R 2013 *Phys. Scripta* **T156** 014075
[227] Lepson J K, Beiersdorfer P, Bitter M, Roquemore A L, Hill K and Kaita R 2015 *J. Phys. Conf. Ser.* **in press** xxx
[228] Beiersdorfer P, Knapp D, Marrs R E, Elliott S R and Chen M H 1993 *Phys. Rev. Lett.* **71** 3939
[229] Beiersdorfer P, Osterheld A L, Scofield J H, Crespo López-Urrutia J R and Widmann K 1998 *Phys. Rev. Lett.* **80** 3022
[230] Beiersdorfer P, Träbert E, Brown G V, Clementson J, Thorn D B, Chen M H, Cheng K T and Sapirstein J 2014 *Phys. Rev. Lett.* **112** 233003
[231] Brandau C, Kozhuharov C, Müller A, Shi W, Schippers S, Bartsch T, Böhm S, Böhme C, Hoffknecht A, Knopp H, Grün N, Scheid W, Steih T, Bosch F, Franzke B, Mokler P H, Nolden F, Steck M, Stöhlker T and Stachura Z 2003 *Phys. Rev. Lett.* **91** 073202
[232] Winters D F A, Vogel M, Segal D M, Thompson R C and Nörtershäuser N C 2007 *Can. J. Phys.* **85** 403